Lethality of SARS-CoV-2 infection in K18 human angiotensin converting enzyme 2 transgenic mice

Authors: Fatai S. Oladunni[1 §], Jun-Gyu Park[1 §], Paula Pino Tamayo[1 §], Olga Gonzalez[1 §], Anwari Akhter[1 §], Anna Allué-Guardia[1 §], Angélica Olmo-Fontánez[1,2], Shalini Gautam[1], Andreu Garcia-Vilanova[1], Chengjin Ye[1], Kevin Chiem[1,2], Colwyn Headley[1], Varun Dwived[1]i, Laura M. Parodi[1], Kendra J. Alfson[1], Hilary M. Staples[1], Alyssa Schami[1,2], Juan I. Garcia[1], Alison Whigham[1], Roy Neal Platt II[1], Michal Gazi[1], Jesse Martinez[1], Colin Chuba[1], Stephanie Earley[1], Oscar H Rodriguez[1], Stephanie Davis Mdaki[1], Katrina N Kavelish[1], Renee Escalona[1], Cory R. A. Hallam[1], Corbett Christie[1], Jean L. Patterson[1], Tim J. C. Anderson[1], Ricardo Carrion Jr[1], Edward J. Dick Jr[1], Shannan Hall-Ursone[1], Larry S. Schlesinger[1], Deepak Kaushal[1], Luis D. Giavedoni[1], Xavier Alvarez[1], Joanne Turner[1,*], Luis Martinez-Sobrido[1,*] and Jordi B. Torrelles[1,*]

Affiliations: [1]Texas Biomedical Research Institute, San Antonio, TX, 78227, USA, and [2]Integrated Biomedical Sciences Program, University of Texas Health Science Center at San Antonio, TX, 78229, USA.

§ Authors contributed equally in this study

***Corresponding authors:** Dr. Luis Martinez-Sobrido, lmartinez@txbiomed.org; Dr. Jordi B. Torrelles, jtorrelles@txbiomed.org; and Dr. Joanne Turner, joanneturner@txbiomed.org.

Keywords: COVID-19, SARS-CoV-2, SARS-CoV-1, hACE2 protein, mouse model, infectivity, chemokine and cytokine storm

ABSTRACT

Vaccine and antiviral development against SARS-CoV-2 infection or COVID-19 disease currently lacks a validated small animal model. Here, we show that transgenic mice expressing human angiotensin converting enzyme 2 (hACE2) by the human cytokeratin 18 promoter (K18 hACE2) represent a susceptible rodent model. K18 hACE2-transgenic mice succumbed to SARS-CoV-2 infection by day 6, with virus detected in lung airway epithelium and brain. K18 ACE2-transgenic mice produced a modest TH1/2/17 cytokine storm in the lung and spleen that peaked by day 2, and an extended chemokine storm that was detected in both lungs and brain. This chemokine storm was also detected in the brain at day 4. K18 hACE2-transgenic mice are, therefore, highly susceptible to SARS-CoV-2 infection and represent a suitable animal model for the study of viral pathogenesis, and for identification and characterization of vaccines (prophylactic) and antivirals (therapeutics) for SARS-CoV-2 infection and associated severe COVID-19 disease.

INTRODUCTION

Human angiotensin-converting enzyme 2 (hACE2) protein is the functional receptor used by severe acute respiratory syndrome coronavirus 1 (SARS-CoV-1) to gain entry to cells.[1,2] Recently hACE2 has also been described as the receptor for acute respiratory syndrome coronavirus 2 (SARS-CoV-2),[3-5] the etiological agent responsible for coronavirus disease 2019 (COVID-19). SARS-CoV-2 emerged in the city of Wuhan, China, in December 2019, causing a pandemic that has dramatically impacted public health and socioeconomic activities across the world.[6-10] Importantly, hACE2 is widely expressed in the lung, central nervous system, cardiovascular system, kidneys, gut, and adipose tissues where it negatively regulates the renin-angiotensin system, and facilitates amino acid transport.[5]

K18 hACE2 transgenic mice [B6.Cg-Tg(K18-ACE2)2Prlmn/J] are susceptible to SARS-CoV-1 infection [11] and recent reports suggest that K18 hACE2 transgenic mice can also be infected with SARS-CoV-2.[12,13] hACE2 expression in K18 hACE2 transgenic mice is driven by the human cytokeratin 18 (K18) promoter.[11] Importantly, hACE2 expression in K18 hACE2 transgenic mice is observed in airway epithelial cells where SARS-CoV-1 and SARS-CoV-2 infections are typically initiated. Recent research indicates that hACE2-expressing mice are useful for studies related to SARS-CoV-2 pathogenesis and COVID-19.[12-16] A validated rodent model of SARS-CoV-2 infection could help to accelerate testing of vaccines (prophylactic) and antivirals (therapeutic) for the prevention and treatment, respectively, of SARS-CoV-2 infection and associated severe COVID-19 disease. Compared to large animals, a murine model would have desirable features of tractability, ease of use and availability, be cost efficient and permit mechanistic studies to identify attributes of severe COVID-19 outcomes in some but not all people who are infected.

Transgenic mice expressing hACE2 have been developed using various promoters that produce mild to moderate SARS-CoV-2 infection in a variety of organs, in addition to physiological (weight

loss, interstitial pneumonia) or immunological (anti-spike IgG) changes.[12-16] No transgenic mice models to date have led to SARS-CoV-2 infection-induced mortality.[15] Adenovirus-based delivery of hACE2 (Ad4-hACE2) to wild-type (WT) C57BL/6 mice resulted in susceptibility to SARS-CoV-2 infection but not mortality.[13,15] K18 hACE2 transgenic mice have previously been shown to represent a good animal model for SARS-CoV-1 infection and associated disease.[11] However, the susceptibility of K18 hACE2 transgenic mice to succumb to SARS-CoV-2 infection has not yet been fully determined.

In this study, we infected K18 hACE2 transgenic mice with SARS-CoV-2 to assess the feasibility of its use as an animal model of SARS-CoV-2 infection and associated COVID-19 disease. Contrary to other constitutively or transiently expressing hACE2 mouse models,[12-19] K18 hACE2 transgenic mice were highly susceptible to SARS-CoV-2 infection, with all mice rapidly losing weight and succumbing to viral infection by 5-6 days post-infection (DPI). Importantly, morbidity and mortality correlated with SARS-CoV-2 replication in the nasal turbinates, lungs and brains at 2- and 4-DPI. Notably, susceptibility was highly associated with a local and systemic chemokine storm, mild to moderate tissue pathology that included vasculitis, and the presence of SARS-CoV-2 nucleocapsid protein (NP) antigen and hACE2 expression in the nasal turbinates and lung epithelium. In contrast, WT C57BL/6 mice survived viral infection with no changes in body weight and undetectable viral replication, NP antigen and hACE2 expression. Altogether, our data provide evidence that K18 hACE2 transgenic mice represent an excellent animal model of SARS-CoV-2 infection and associated severe COVID-19 disease, providing the research community with a much needed small animal model to evaluate vaccines and/or antivirals for SARS-CoV-2 infection and associated severe COVID-19 disease *in vivo*.

MATERIALS AND METHODS

Ethics statement

All experimental procedures with animals were approved by the Texas Biomedical Research Institute (Texas Biomed) Institutional Biosafety Committee (IBC, #20-004 and #20-010) and Institutional Animal Care and Use Committee (IACUC, #1708 MU) and under Biosafety Level 3 (BSL3) and animal BSL3 (ABSL3) facilities at Texas Biomed.

Virus, cells and viral propagation

SARS-CoV-2, USA-WA1/2020 strain (Gen Bank: MN985325.1), was obtained from BEI Resources (NR-52281). SARS-CoV-2 USA-WA1/2020 was isolated from an oropharyngeal swab from a patient with a respiratory illness in January 2020 in Washington, US. The virus stock obtained from BEI Resources was a passage (P)4 stock, and was used to generate a master P5 seed stock. The P5 stock was used to generate a P6 working stock. P5 and P6 stocks of SARS-CoV-2 were generated by infecting at low multiplicity of infection (MOI, 0.001) Vero E6 cells obtained from the American Type Culture Collection (ATCC, CRL-1586). At 72 h post-infection, tissue culture supernatants (TCS) were collected and clarified before being aliquoted and stored at -80°C. Standard plaque assays (plaque forming units, PFU/ml) in Vero E6 cells were used to titrate P5 ($1.7x10^6$ plaque forming units, PFU/ml) and P6 ($2.6x\ 10^6$ PFU/ml) viral stocks.

Mice

Specific-pathogen-free, 4-5-weeks-old, female and male B6.Cg-Tg(K18-ACE2)2Prlmn/J (Stock No: 034860, K18 hACE2) hemi-zygotes, or wild-type (WT) C57BL/6 control mice, were purchased from The Jackson Laboratory (Bar Harbor, ME). K18 hACE2 transgenic and WT C57BL/6 mice were identically maintained in micro-isolator cages at Animal Biosafety Level (ABSL)-2 for noninfectious studies, or at ABSL-3 for studies involving SARS-CoV-2. Mice were provided sterile

129 water and chow *ad libitum* and acclimatized for at least one week prior to experimental
130 manipulation.
131
132 Based on the limited number of K18 hACE2 transgenic mice from The Jackson Laboratory, n=3
133 each for female and male mice were used for morbidity and mortality studies, while n=4 each for
134 female and male mice were used for viral titers at 2- and 4-DPI, respectively. An n=3 each for
135 female and male K18 hACE2 transgenic mice were used as mock-infected controls in the
136 morbidity and mortality studies, and 1 male and 1 female for all other studies. Equal numbers of
137 matched female and male WT C57BL/6 control mice were used in this study.
138
139 **Mouse infection and sample processing**
140 Female (n=3) and male (n=3) K18 hACE2 transgenic and WT C57BL/6 mice were either mock
141 (PBS)-infected (controls) or infected intranasally (i.n.) with 10^5 PFU of SARS-CoV-2 in a final
142 volume of 50 µl following isoflurane sedation. Limited numbers of available K18 hACE2 transgenic
143 mice reduced the study to a single exposure dose of SARS-CoV-2. After viral infection, mice were
144 monitored daily for morbidity (body weight) and mortality (survival). Mice showing more than 25%
145 loss of their initial body weight were defined as reaching experimental end-point and humanely
146 euthanized. In parallel, K18 hACE2 transgenic or WT C57BL/6 female (n=8) and male (n=8) mice
147 were infected and euthanized at days 2 (n=4/sex) or 4 (n=4/sex) DPI. Ten tissues (nasal turbinate,
148 trachea, lung, heart, kidney, liver, spleen, small intestine, large intestine, and brain) were
149 harvested from each mouse. Half organ was fixed in 10% neutral buffered formalin solution for
150 molecular pathology analyses and the other half was homogenized in 1mL of PBS using a
151 Precellys tissue homogenizer (Bertin Instruments) for viral titration. Tissue homogenates were
152 centrifuged at 21,500 x *g* for 5 min and supernatants were collected for measurement of viral load
153 and chemokine/cytokine analyses.
154

155 **Measurement of viral loads**

156 Confluent monolayers of Vero E6 cells (96-well plate format, 4 x 10^4 cells/well, duplicates) were
157 infected with 10-fold serial dilutions of supernatants obtained from the organ homogenates. Virus
158 was adsorbed for 1 h at 37°C in a humidified 5% CO_2 incubator. After viral adsorption, cells were
159 washed with PBS and incubated in post-infection media containing 1% microcrystalline cellulose
160 (Avicel, Sigma-Aldrich). Infected cells were incubated in a humidified 5% CO_2 incubator at 37°C
161 for 24 h. After viral infection, plates were inactivated in 10% neutral buffered formalin
162 (ThermoFisher Scientific) for 24 h. For immunostaining, cells were washed three times with PBS
163 and permeabilized with 0.5% Triton X-100 for 10 min at room temperature. Cells were then
164 blocked with 2.5% bovine serum albumin (BSA) in PBS for 1 h at 37°C, followed by incubation
165 with 1 µg/ml of a SARS-CoV-1 NP cross-reactive monoclonal antibody (MAb), 1C7, diluted in 1%
166 BSA for 1 h at 37°C. After incubation with the primary NP MAb, cells were washed three times
167 with PBS, and developed with the Vectastain ABC kit and DAB Peroxidase Substrate kit (Vector
168 Laboratory, Inc., CA, USA) according to the manufacturers' instructions. Viral titers were
169 calculated as PFU/mL.
170
171 **Multiplex cytokine assay**
172 Cytokines and pro-inflammatory markers were measured using a custom 18-multiplex panel
173 mouse magnetic bead Luminex assay (R&D Systems, Mouse 18-Plex, lot L134111), following the
174 manufacturer's instructions. Immunoassays were performed in the ABSL-3 and samples
175 decontaminated by an overnight incubation in 1% formalin solution before readout on a Luminex
176 100/200 System with the following parameters: gate 8,000-16,500, 50 µl of sample volume, 50-
177 100 events per bead, sample timeout 60 seconds, low PMT (LMX100/200: Default).
178
179
180

Interferon (IFN) ELISA

Mouse IFN-α (Type I) and IFN-λ (Type III) were measured by enzyme-linked immunosorbent assays (ELISA) (PBL Assay Science) following the manufacturer's recommendations, detecting all 14 known IFN-α subtypes and IFN-λ 2 and 3.

Histopathology analyses

Tissues were fixed in 10% neutral buffered formalin, embedded in paraffin blocks, and sectioned at 4μm thickness. Sections were stained with Haemotoxylin and Eosin (H&E) and evaluated using light microscopy in a blinded manner by a board certified veterinary pathologist.

Immunohistochemistry assays

Immunostaining and confocal microscopy were performed as previously described.[20,21] Briefly, 5 μm tissues sections were mounted on Superfrost Plus Microscope slides, baked overnight at 56°C and passed through Xylene, graded ethanol, and double distilled water to remove paraffin and rehydrate tissue sections. A microwave was used for heat induced epitope retrieval (HIER). Slides were boiled for 20 min in a TRIS-based solution, pH 9.0 (Vector Labs H-3301), containing 0.01% Tween-20. Slides were briefly rinsed in distilled hot water, and transferred to a hot citrate based solution, pH 6.0 (Vector Labs H-3300) and cooled to room temperature. Once cool, slides were rinsed in TRIS buffered saline (TBS) and placed in a black, humidifying chamber and incubated with Background Punisher (Biocare Medical BP974H) for 40 minutes. Subsequently, slides were stained with primary rabbit antibodies against the following proteins: SARS-CoV-1 NP at 1:4,000 dilution (a rabbit polyclonal antibody shown to cross-react with SARS-CoV-2 NP), hACE2 receptor (hACE2 Recombinant Rabbit Monoclonal Antibody, 1:50, Thermo-Fisher, Cat#SN0754) and DAPI nuclear stain (1:20,000, Invitrogen, Carlsbad, CA). The primary antibodies were detected with goat anti-rabbit-AP developed with Permanent Red warp (mach3 Biocare Medical).

206 **Statistical analysis**

207 Statistical significance was determined using Prism 8 software (GraphPad Software, San Diego,
208 CA). The unpaired, two-tailed Student's *t*-test was used for two group comparisons for each time-
209 point and reported as *$p< 0.05$; **, $p< 0.005$; ***, $p< 0.0005$. For individual cytokine/chemokine
210 analyses, correlations were made between analyte concentrations [measured as the area under
211 the curve (AUC) or the peak concentration] and viremia using linear regression by hierarchically
212 clustered Pearson test. Multiple comparisons among groups and/or time-points were analyzed
213 using one-way ANOVA with Tukey's post-test and reported as §, $p< 0.05$; § §, $p< 0.005$; § § §
214 , $p< 0.0005$.
215
216
217
218
219
220
221
222
223
224
225
226
227
228
229
230

RESULTS

K18 hACE2 transgenic mice are susceptible to SARS-CoV-2 infection

K18 hACE2 transgenic and WT C57BL/6 mice where i.n. mock-infected (PBS), or infected with $1x10^5$ PFU of SARS-CoV-2, USA-WA1/2020 strain, and followed for body weight loss and survival for 14 days. Because of the limited number of K18 hACE2 transgenic mice provided by The Jackson Laboratory, 3 female and 3 male mice per group were used for body weight and survival studies while 4 female and 4 male mice per group were used for viral titers, chemokine/cytokine, histopathology and immunohistochemistry analyses at 2 and 4 DPI. The mock-infected groups included 3 female and 3 male mice. The same matched groups of WT C57BL/6 female and male mice were included in this experiment.

By 5-DPI, SARS-CoV-2 infected K18 hACE2 transgenic mice lost over 20% of their initial body weight, were lethargic with rough fur and hunched appearance, immobile, and did not eat or drink, and succumbed to the infection by 6-DPI (**Figs 1A, B**). All K18 hACE2 transgenic mice succumbed to infection by 6-DPI, with the exception of one that was humanely euthanized due to IACUC-defined endpoints. Mock-infected K18 hACE2 transgenic or WT C57BL/6 mice, or SARS-CoV-2 infected WT C57BL/6 mice appeared healthy, maintained weight, and all survived SARS-CoV-2 infection for the duration of this study (**Figs 1A, B**). Differentiating by sex, we observed that SARS-CoV-2 infected male K18 hACE2 transgenic mice lost weight starting 1-DPI, at the rate of approximately 5% per day whereas SARS-CoV-2 infected female K18 hACE2 transgenic mice did not begin to lose weight until 3-DPI (**Fig S1**). In both cases, after 3-DPI, morbidity indicators accelerated until all K18 hACE2 transgenic mice, independent of sex, succumbed to SARS-CoV-2 infection by 6-DPI (**Fig S1**).

To correlate body weight loss (**Fig. 1A**) and survival (**Fig. 1B**) with viral replication, female (n=8) and male (n=8) K18 hACE2 transgenic and WT C57BL/6 mice were similarly mock-infected or

infected with $1x10^5$ PFU of SARS-CoV-2 and euthanized at 2- or 4-DPI, to determine viral titers in the nasal turbinate, trachea, lung, heart, kidney, liver, spleen, small intestine, large intestine, and brain. By 2-DPI, K18 hACE2 transgenic mice had ~$1x10^3$ PFU in nasal turbinate and ~$1x10^4$ PFU in lung, indicating the presence of SARS-CoV-2 in both the upper and lower respiratory tracts. Viral titers at both sites were maintained at 4-DPI (**Figs 1C, D**). SARS-CoV-2 was also detected in the brain at 4-DPI (~$1x10^3$ PFU) (**Fig 1E**), but absent in all other organs. In all organs where SARS-CoV-2 was detected (nasal turbinate, lung and brain), we observed no sex differences in viral titers (**Fig S2**). SARS-CoV-2 infected WT C57BL/6 mice had undetectable viral loads at both DPI in all organs studied, in accordance with previous studies suggesting that WT C57BL/6 mice are resistant to SARS-CoV-2 infection (**Figs 1A-E, S1 and S2**).[15] Taken together, these results demonstrate the susceptibility of K18 hACE2 transgenic mice, but not WT C57BL/6 mice, to SARS-CoV-2 infection at the studied MOI, with detectable virus in the upper and lower respiratory tract, and brain, at early time points post-infection.

SARS-CoV-2 infection of K18 hACE2 transgenic mice drives a local and systemic chemokine storm

An early (2-DPI) chemokine storm was observed in the lungs of K18 hACE2 transgenic mice infected with SARS-CoV-2 (**Fig 2A**). MIP-2/CXCL2, MCP-1/CCL2, MIP-1α/CCL3, MIP-1β/CCL4, RANTES/CCL5 and IP-10/CXCL10 levels were significantly increased in the lungs relative to C57BL/6 WT infected mice or mock-infected K18 hACE2 transgenic mice. At 4-DPI several chemokines had decreased in magnitude but were significantly elevated when compared to C57BL/6 WT or mock-infected K18 hACE2 transgenic mice. For some chemokines, such as RANTES/CCL5, the high levels detected in the lung at 2-DPI were sustained at 4-DPI (**Fig 2A**). Chemokine levels in the lungs of C57BL/6 WT mice did not increase in response to SARS-CoV-2 infection at either time point tested. A chemokine storm has been described in humans with

COVID-19 disease, and it has been associated with development of acute respiratory distress syndrome (ARDS) in mice.[22]

As a measure of systemic inflammation, we determined chemokine levels in the spleen, where MIP-2/CXCL2, IP-10/CXCL10, MIP-1α/CCL3, and MIP-1β/CCL4 were significantly increased at 2-DPI (**Fig 2B**). Only MIP-1α/CCL3 and MIP-1β/CCL4 maintained a significant increase at 4-DPI when compared to both mock-infected K18 hACE2 transgenic mice and WT-infected C57BL/6 mice. Contrary to the lung, we did not observe an increase in RANTES/CCL5 relative to virus-infected C57BL/6 WT or mock-infected K18 hACE2 transgenic mice (**Fig 2B**), identifying a potential sustained lung-specific chemokine response after SARS-CoV-2 infection. Our results indicate that SARS-CoV-2 infection of K18 hACE2 transgenic mice triggers both a local (lung) and systemic (spleen) chemokine storm. Chemokine analysis in nasal turbinate supported the early chemokine storm at 2-DPI in SARS-CoV-2 infected K18 hACE2 transgenic mice, with significant but transient high levels of MCP-1/CCL2, MIP-1α/CCL3, RANTES/CCL5 and IP-10/CXCL10 (**Fig S3A**). No differences were observed in the trachea (**Fig S3B**). Interestingly, the brain of SARS-CoV-2 infected K18 hACE2 transgenic mice also had significant levels of MIP-2/CXCL2, IP-10/CXCL10 and MIP-1α/CCL3 but in contrast to other organs, these were detectable only at 4-DPI (**Fig 2C**), similar to the detection of virus in brain. There were no differences in chemokine levels in the lung between male and female K18 hACE2 transgenic infected mice, with the exception of IP-10/CXCL10 at 2-DPI, which was significantly higher in female K18 hACE2 transgenic mice (**Fig S5A**).

SARS-CoV-2 infection of K18 hACE2 transgenic mice drives a local cytokine storm

We next determined if SARS-CoV-2 infection of K18 hACE2 transgenic mice resulted in a cytokine storm, as described during the development of severe COVID-19 disease in humans (reviewed

in [22-26]). Multiple tissues were analyzed to define local and systemic inflammatory, TH1, TH17, and TH2 responses. At 2-DPI the cytokine profile in the lungs of K18 hACE2 transgenic mice included a mixed inflammatory (TNF, IL-6, IFN-α, and IFN-λ), TH1 (IL-12, IFN-γ), TH17 (IL-17, IL-27) and TH2 (IL-4, IL-10) profile (**Fig 3A**). Notably, IL-1β production was absent at 2- and 4-DPI. Reports in humans with COVID-19 showed that IL-1 precedes other cytokine production [26,27] Thus, studying earlier time points may have been informative in this mouse model with regard to IL-1β production.

Similar to that observed for chemokines, the cytokine storm resolved by 4-DPI with the exception of TNF and the type I and III IFNs which remained significantly increased when compared to SARS-CoV-2 infected C57BL/6 WT or mock-infected K18 hACE2 transgenic mice (**Fig 3A**). Reduction of chemokines and cytokines occurred despite increasing viral loads and extensive weight loss in virus-infected K18 hACE2 transgenic mice. No significant sex differences were found for cytokine levels in the lung (data not shown).

With few exceptions, the cytokine storm was absent in the spleen (**Fig 3B**), nasal turbinate (**Fig S4A**), and trachea (**Fig S4B**) of SARS-CoV-2 infected K18 hACE2 transgenic mice, indicating that the cytokine response was relatively localized to the lung. Exceptions included an increase in TNF at 2-DPI in the spleen (**Fig 3B**), and a moderate but significant increase in IL-10 in the nasal turbinate at 2-DPI (**Fig S4A**). Interestingly, although we observed decreased cytokines in the lung by 4-DPI, some TH1 and TH17 cytokines (**Fig 3C**) and chemokines (**Fig 2C**) increased in the brain at this same time-point, suggesting a delayed viral spread to the brain. IL-1β, IL-27, IL-4, IL-13 and IL-10 were also elevated in the brain of C57BL/6 WT mice infected with SARS-CoV-2, even in the absence of detectable virus in any organs. IFN-α (type I) was not detected in the brain of SARS-CoV-2-infected K18 hACE2 transgenic or WT C57BL/6 mice. However, both

IFN-γ (type II) and IFN-λ (type III) were lower in K18 hACE2 transgenic mice relative to WT C57BL/6 mice infected with SARS-CoV-2, and similar to mock-infected K18 hACE2 transgenic mice (**Fig 3C**).

A clear sex difference was observed in the brain. Males had significantly higher TH1 and TH17 cytokine responses at 4-DPI compared to SARS-CoV-2 infected female K18 hACE2 transgenic mice, and female mice had significantly higher TH2 responses when compared to male K18 hACE2 transgenic mice at the same time point (**Fig S5B**). These sex differences are similar to studies of acute LPS-induced inflammation.[28,29] The TH1/TH2 sex difference was not observed in C57BL/6 WT mice infected with SARS-CoV-2 (**Fig S5B**).

We further assessed correlations between viral titers, chemokines and cytokines observed in each tissue, and performed hierarchical clustering to identify the immune response characteristics in response to SARS-CoV-2 infection in K18 hACE2 transgenic mice (**Figs 4A-C and Figs S6A, B)**. At 2-DPI in the lungs of SARS-CoV-2 infected K18 hACE2 transgenic mice we observed two distinct clusters (**Fig 4A**): A cytokine cluster defined by the presence of IL-10 (Cluster-1, **Fig 4A**), which correlated with the presence of IL-4 (0.94), IL-6 (0.91), IL-13 (0.91) and IL-12p70 (0.86); and a chemokine cluster (Cluster-2, **Fig 4A**) defined by MCP-1/CCL2 and correlating with the presence of MIP-1β/CCL4 (0.99), MIP-2/CXCL2 (0.95) and MIP-1α/CCL3 (0.93), and cytokines TNF (0.95) and IFN-γ (0.93). Lung viral loads did not correlate with the presence of any specific cytokine or chemokine, possibly due to the variability seen for viral loads and a quickly progressing disease. The 2-DPI correlative clusters in the lung were not maintained at 4-DPI but other smaller clusters were observed, the largest being led by IL-13 (Cluster-3, **Fig 4A**) correlating with IL1-β (0.97) and IL-4 (0.93), suggestive of a rapidly developing immune response similar in nature, but not form, to the cytokine storm observed in humans.[22-26]

The IL-10 cluster (Cluster-1) was also observed in the spleen at 2-DPI, correlating with IL-6 (0.96), IL-4 (0.95), IL-13 (0.93) and IL-1β (0.88); and at 4-DPI, correlating with IL-13 (0.92), IL-4 (0.89) and IL-1β (0.76)] (**Fig 4B**), but not in the brain (**Fig 4C**). Indeed, in the brain a correlation between IL-2, IL-4 and IL-13 was observed independent of IL-10 at 2-DPI (Cluster-4, **Fig 4C**). In the brain, a larger cluster (Cluster 5) was observed at 4-DPI, driven by RANTES/CCL5 and correlating with all MCP-1/CCL2, MIP-1α/CCL3, TNF (0.99) and IL-6 (0.98) (**Fig 4C**). Nasal turbinate and trachea did not have significantly elevated levels of cytokines and chemokines (**Fig S6 A, B).**

When analyzed by sex, Cluster-1 (**Fig 4A**) had perfect correlations in males at 2-DPI but these correlations were absent in females with the exception of the IL-4 correlation with IL-10 (0.95) (**Fig S7A**). Cluster-2 in males at 2-DPI did not extend to 4-DPI for either sex (**Fig S7B**). Indeed, at 4-DPI in males, a new Cluster-9 with correlations between TNF, MCP-1/CCL2 and MIP-1α/CCL3 together with IL-12p70 and MIP-2/CXCL2 was observed (**Fig S7B**).

In the brain, RANTES/CCL5, MIP-1α/CCL3 and IL-10 correlated with SARS-CoV-2 viral load in the nasal turbinate at 2-DPI only in males (**Fig S7C**). This correlation disappeared at 4-DPI but a correlation between SARS-CoV-2 viral load and IL-10 in the brain was then observed (**Fig S7D**). Conversely, SARS-CoV-2 viral load in the brain positively correlated with the presence of chemoattractants [MIP-2/CXCL2, IP-10/CXCL10, MCP-1/CCL2 and MIP-1α/CCL3] in females (**Fig S7D**). All correlated with the presence of RANTES/CCL5 and TNF in the brain, as well as with SARS-CoV-2 viral titers in nasal turbinate (**Fig S7D).**

SARS-CoV-2 infected K18 hACE2 transgenic mice develop rhinitis, pneumonia with associated pulmonary inflammation

WT C57BL/6 mice developed minimal mononuclear and neutrophilic interstitial pneumonia (lung) (**Figs 5A, B, bracket**) and rhinitis (nasal turbinate) (data not shown) that dissipated by 4-DPI (**Figs 5C**, **D**), with very few consistent changes in other tissues with the exception of lymphocyte aggregates in the lamina propria of the small intestine (**Fig 5I, asterisk**) and few small aggregates of mixed mononuclear inflammation with few neutrophils occasionally admixed with individual hepatocellular necrosis (**Fig 5J, arrowhead**). Minimal alveolar histiocytosis (**Fig 5D, asterisk**), pneumocyte type II cells (**Fig 5D**, **arrowheads**), perivascular mononuclear inflammation (**Fig 5D, bracket**) and rhinitis with low numbers of neutrophils (**Fig 5K, arrowhead**) were variably observed in 4-DPI WT C57BL/6 mice (**Fig 5D**). Brain tissue from SARS-CoV-2-infected C57BL/6 WT mice 4-DPI was normal (**Fig 5L**). Thus, WT C57BL/6 mice had minimal to no pathologic findings consistent with their undetectable viral loads.

K18 hACE2 transgenic mice developed rhinitis (data not shown), and interstitial pneumonia (**Figs 5E, F**) associated with alveolar histiocytosis admixed neutrophils and lymphocytes (**Fig 5F, asterisks**), mild type II pneumocyte hyperplasia (**Fig 5F, arrowhead**), bronchiolar syncytia (**Fig 5F, arrow**), endothelial cell hyperplasia and vasculitis (**Fig 5F, bracket**) by 2-DPI. Mice showed evidence of liver inflammation, although mixed inflammatory aggregates were minimal with variable amounts of individual hepatocellular necrosis (**Fig 5N, arrowhead**), as well as gut associated lymphoid tissue (GALT) with prominent centers (**Fig 5M, asterisk**). By 4-DPI, the majority of K18 hACE2 transgenic mice had 25% or greater lung involvement indicative of pneumonia (**Fig 5G**), with affected areas presenting with inflammatory cellular accumulations and hemorrhage in alveolar spaces (**Fig 5H, asterisk**) and interstitium (**Fig 5H, bracket**), intra-alveolar fibrin admixed cellular debris (**Fig 5H, arrow**), vasculitis (**Fig 5H, bracket**), edema (**Fig 5H, arrowhead**), and neutrophilic rhinitis (**Fig 5O, bracket**). By 4-DPI, K18 hACE2 transgenic

mice had inflammation in the liver (not shown), and lymphocyte and neutrophil aggregates in the small intestine (not shown). Two K18 hACE2 transgenic mice had evidence of cerebral pathology; one animal had perivascular hemorrhage (not shown) and another animal had mild meningoencephalitis with vasculitis (**Fig 5P, arrowhead**).

SARS-CoV-2 NP and hACE2 expression in tissues of SARS-CoV-2 infected K18 hACE2 transgenic mice

Immunohistochemistry (IHC) labeling for SARS-CoV-2 NP antigen showed a heterogeneous distribution of viral NP in the lungs of K18 hACE2 transgenic mice; however, this distribution was more focalized in the nasal turbinate (**Fig 6A**). Virus NP antigen was undetectable in all organs from C57BL/6 WT-infected mice (**Fig 6A**). Distribution of the hACE2 receptor by IHC was obvious in the lungs and in the epithelium of the nasal turbinate of K18 hACE2 transgenic mice (**Fig 6A**) and, as expected, absent from C57BL/6 WT mice (**Fig 6A**). Viral NP antigen did not co-localize in the same regions as hACE2 except in the lung (**Fig. 6A** and data not shown) perhaps because necropsies were first performed at 2-DPI. hACE2 was also highly expressed in the choroid plexus and some cells were also positive for SARS-CoV-2 NP (**Fig 6B**). This result opens the possibility that the cerebral spinal fluid (CSF) produced by the choroid plexus, could carry the virus into the central nervous system, disseminating SARS-CoV-2 through the body to the points of CSF reabsorption.

DISCUSSION

Herein we demonstrate that K18 hACE2 transgenic mice are highly susceptible to SARS-CoV-2 infection, quickly reaching study endpoints by 6-DPI following i.n. infection with 10^5 PFU. SARS-CoV-2 was detected in the nasal turbinate and lung of K18 hACE2 transgenic mice on 2- and 4-DPI, and in the brain at 4-DPI. The existence of SARS-CoV-2 in the lung, nasal turbinate and brain of SARS-CoV-2-infected hACE2 transgenic mice was verified by the presence of NP antigen using IHC, although NP antigen did not generally co-localize with hACE2 protein expression except in lungs, perhaps because SARS-CoV-2 had already entered the epithelium of the nasal turbinate and other tissues by 2-DPI. K18 hACE2 transgenic mice developed progressive pneumonia and by 4-DPI there was evidence of intra-alveolar fibrin, cellular debris, vasculitis and edema in the lung, likely driving morbidity and mortality. SARS-CoV-2 infection of K18 hACE2 transgenic mice was also associated by a marked significant increase in chemokine and cytokine production in the lung and spleen by 2-DPI. Although most chemokines and cytokines expression levels were reduced by 4-DPI, MCP-1/CCL2 and IFN-λ remained elevated in the lung and virus persisted.

An important distinction between our study and others is that K18 hACE2 transgenic mice succumbed to SARS-CoV-2 infection by 6-DPI when infected at 10^5 PFUs. This phenotype has not been reported in any other mouse studies of SARS-CoV-2 infection,[12-19] including a study using ~10^5 PFU (i.n.) of the Hong Kong/VM20001061/2020 SARS-CoV-2 strain.[12] K18 hACE2 transgenic mice express the hACE2 protein under the human K18 promoter, which induces high transgene expression specifically in airway epithelial cells.[11,30] The K18 hACE2 transgenic mice contain 2.5 kb of the K18 genomic sequence, including the promoter, first intron, and a translational enhancer (TE) sequence from alfalfa mosaic virus upstream of hACE2, followed by exons 6-7 and the poly(A) signal of the human K18 gene. This complete 2.5 kb K18 genomic

458 sequence is necessary for the K18 hACE2 transgene expression in lung airway epithelium, and
459 other organs such as the liver, kidney and gastrointestinal tract.[11,31] This contrasts with mice
460 expressing hACE2 under the mouse ACE2 promoter.[14,16,19,32] Thus, a potential difference in
461 results between our study and others is the high expression levels of hACE2 in the airway epithelia
462 in the K18 hACE2 transgenic mouse model used in this study. This concept is further supported
463 by our IHC data showing higher levels of hACE2 expression in the airway epithelium (nasal
464 turbinate and lung, **Fig 6**) in K18 hACE2 transgenic mice. Of interest, other studies infected the
465 K18 hACE2 transgenic mice with a lower MOI (10^4 PFUs) than used in this present study, wherein
466 the majority of mice showed morbidity by 7-DPI but not mortality.[12,13] However, when K18 hACE2
467 transgenic mice were infected with 10^5 PFU in those studies, they developed progressive weight
468 loss and lung pathologies at 2-DPI and central nervous system (CNS) involvement by 6-DPI, 2-
469 days later than our observations ([31], *Perlman S, McCray, personal communication, June 2020*).
470 Thus, in addition to the presence of hACE2 on the upper and lower respiratory tract epithelium
471 for establishing SARS-CoV-2 infection in K18 hACE2 transgenic mice, it appears that the number
472 of viral particles during the initial exposure is also a critical determinant of developing severe
473 COVID-19 morbidity and mortality in this model, similar to the situation with other respiratory viral
474 infections (e.g. influenza).[33]
475
476 The term cytokine storm was first used during avian H5N1 and 1918 influenza virus infections, for
477 SARS-CoV-1 and, more recently, for SARS-CoV-2.[27,34-36] In K18 hACE2 transgenic mice, we
478 observed correlations between cytokines, the presence of virus, SARS-CoV-2 NP antigen, and
479 pathogenesis (histopathology). As observed in our study, as well as reported in mice expressing
480 hACE2 under a mouse or adenovirus promoter,[12-19] it appears that the magnitude of cytokine and
481 chemokine responses during SARS-CoV-2 infection is another important determinant of disease
482 severity and this result may be applicable to predicting a person's clinical outcome after SARS-
483 CoV-2 infection [asymptomatic, mild COVID-19 or severe COVID-19 Acute Respiratory Distress

Syndrome (CARDS)]. K18 hACE2 transgenic mice expressed an early (2-DPI) and mixed cytokine profile that included pro-inflammatory, TH1, TH2 and TH17 cytokines indicative of cytokine dysregulation in the lungs. This cytokine storm resolved by 4-DPI, even though mice were reaching a moribund state, with the exception of TNF and the type I and III IFNs which remained significantly increased. These results suggest that TNF and type I and III IFN's may be important drivers of disease progression.

While the amount of chemokines decreased at 4-DPI, MCP-1/CCL2 remained elevated indicative of ongoing tissue damage and cellular recruitment. MCP-1/CCL2 and IP-10/CXCL10 were produced at high levels in K18 hACE2 transgenic mice after SARS-CoV-2 infection, both, locally and systematically at 2-DPI, as well as in the brain at 4-DPI. Elevated MCP-1/CCL2 and IP-10/CXCL10 likely explained the accumulation of inflammatory cells in the lung including the observed neutrophils and monocytes (**Table 1**), and development of vasculitis that likely contributed to morbidity and mortality. In this context, gene expression signatures in the lungs of SARS-CoV-2-infected patients who succumb to viral infection showed high expression of MCP-1/CCL2 and IP-10/CXCL10, which was linked to type I and II IFN responses.[34,37] Early reports from COVID-19 patients also indicates that chemokines are elevated[27] and MCP-1/CCL2 and IP-10/CXCL10 have been implicated in COVID-19 patients,[27] demonstrating that K18 hACE2 transgenic mice replicate cytokine and chemokine storm traits observed in humans.

The consequences of reduced cytokine production at 4-DPI is unknown but we can speculate on several modes of action. This process could be driven by accumulation of lymphoid tissue around the airways, which dampens initial responses in severe influenza virus infection.[38] Alternatively, there may be a reestablishment of the balance between pro-inflammatory cytokines and their soluble receptors or inhibitors in the alveolar compartment.[39] The production of TH2 cytokines also represents another mechanism involved in regulating pro-inflammatory responses. The

observed production of IL-10, although commonly recognized as an anti-inflammatory cytokine, plays a role in fibrosis, inducing collagen production and fibrocyte recruitment into the lung.[34,40] In this context, several correlative cytokine clusters linked by IL-10 were observed in multiple organs including the lungs and the brain. Elevated IL-10 can be associated with immune paralysis,[34] altering the function of neutrophils and monocytes reaching the local infection site, potentially driving the expansion of the SARS-CoV-2 infection in the K18 hACE2 transgenic mouse model. Alternatively, the high levels of IL-6 observed in tissues may provide a mechanism for enhancing TNF activity during acute viral infection,[39] as well as B cell antibody production and fibrosis.[41] Thus it is conceivable that if one or more of these regulatory mechanisms are aberrantly regulated or absent, the pro- and anti-inflammatory balance critical for lung immune homeostasis might be disrupted, contributing to the cytokine storm observed in the K18 hACE2 transgenic mouse model upon SARS-CoV-2 infection. Interestingly, IL-4/IL-13 activation of the STAT-6 signaling pathway is associated with some lung pathologies including asthma.[42,43] The IL-6/IL-10/IL-13 correlation has also been described in patients with viral infections, where their expression levels in serum correlates with the disease clinical state,[44] as well as to aortic aneurysm.[45] Indeed, influenza infection is related to heart pathologies.[46]

Although SARS-CoV-2 was detected in the brain at 4-DPI, minimal histopathological changes were observed for the majority of mice, except for two mice that presented with multifocal perivascular neutrophils, lymphocytes, microglial cells and necrotic debris, vasculitis, and inflammation that extended to the meninges with hemorrhage. Brain cytokine responses were dominated by TH2 cytokines (IL-4, IL-13, IL-10, IL-27, and IL-33) which may reflect the natural TH2 status of the brain.[47,48] IL-27 is known to regulate inflammation in the CNS through upregulation of IL-10,[49-51] but can also potentiate inflammation through induction of IL-12.[52] The cytokine profiles observed in SARS-CoV-2 infected mice suggest it is the former response at play, working to counterbalance the potent peripheral TH1 responses. We also observed increases in

cytokine production at 2- and 4-DPI that included a robust IL-1β response. The detection of IL-1β in brain at 2-DPI suggests that virus spread to brain was delayed relative to lung and spleen [27]. Interferon type II and III were significantly lower in the brain of SARS-CoV-2 infected K18 hACE2 transgenic mice when compared to WT C57BL/6 mice at all-time points studied, and interferon type I was not detected, which could be a deciding factor driving colonization of the brain by SARS-CoV-2 in this mouse model. Indeed, deviation from homeostatic IFN type I/IFN type II balance contributes to insufficient immune surveillance of the CNS and loss of immune-dependent protection, or immune-mediated destruction.[53]

Most intriguing was that many TH2 cytokines (IL-1β, IL-27, IL-4, IL-13, IL-33 and IL-10) were also elevated in the brain of WT C57BL/6 control mice at 2- and 4-DPI. Although we did not find any virus in WT C57BL/6 mice, it suggests that the virus might be privy to the blood brain barrier because the cytokine pattern in the brain was similar to K18 hACE2 transgenic mice. C57BL/6 mice express the mouse ACE2 protein and studies have shown that ACE2 gene-disrupted mice are less susceptible to SARS-CoV-1.[54] Therefore, it is possible that endogenous ACE2 in mice could drive a cytokine response in the brain of WT C57BL/6 mice infected with SARS-CoV-2 while showing very limited peripheral responses. Overall, these data suggest that there may be some tropism for SARS-CoV-2 in the brain of WT mice, supporting some reports of neurological issues in humans with COVID-19.[55] We also observed sex differences in K18 hACE2 transgenic mice with males exhibiting a TH1 and TH17 phenotype at 4-DPI whereas female K18 hACE2 transgenic mice had a TH2 responses at the same time point, similar to studies of acute LPS-induced inflammation,[28,29] which suggests that males may be more prone to exhibit neurological problems during SARS-CoV-2 infection, independent of viral load.

While our findings clearly identify the K18 hACE2 transgenic mouse as a model for SARS-CoV-2 infection and COVID-19 disease, our studies have some limitations. The primary limitation was the number of mice that were available for study, due to limited supply from the vendor. We maximized our studies by performing two independent experiments that cross-validated each other in survival and pathogenesis results. Both studies showed considerable sensitivity of K18 hACE2 transgenic mice to SARS-CoV-2 infection. We chose a relatively high viral dose (MOI $1x10^5$ PFU/mouse) that was capable of causing extensive disease, but we were unable to include additional time points to further understand the time course of immune responses (*e.g*. 1-DPI) or whether the chemokine and cytokine storm increased again at study endpoints (*e.g*. 5/6-DPI). Likewise, the limited number of K18 hACE2 transgenic mice did not allow us to use different viral doses to calculate the mouse lethal dose 50 (MLD_{50}) of SARS-CoV-2. Inclusion of WT C57BL/6 control mice in our studies confirmed that mice are not naturally susceptible to infection with SARS-CoV-2 without experimental manipulation to express hACE2, further confirming that hACE2 is the receptor for SARS-CoV-2.[56-59]

Several groups are developing large animal models of SARS-CoV-2 infection and COVID-19, with a primary focus on nonhuman primates (NHP) models. Reports indicate that macaques develop self-limiting disease with a strong anamnestic responses (innate and adaptive)[60-62], while vervets may model signs of acute respiratory distress.[63] These models are necessary for preclinical testing for safety, immunogenicity and efficacy of vaccines and therapeutics. However, no NHP models display the end-stage COVID-19 outcomes that are effectively captured in the K18 ACE2 transgenic mice. Hence, evaluation of therapeutics and antivirals must also leverage transgenic murine models of end-stage lethal COVID-19 disease, characterized by ARDS. The K18 hACE2 mouse model can work in concert with other rodent models, such as the Golden Syrian hamster model,[64-66] to provide two-step testing of therapeutics. This would fill a critical gap and relieve the pressure on the limit number of NHPs available for this purpose worldwide. Moreover, the K18

hACE2 mouse model could also be used to assess the contribution of host cellular factors in SARS-CoV-2 infection or associated COVID-19 disease, for example through crossing K18 hACE2 mice with IFNAR KO mice to assess the contribution of type I IFN in SARS-CoV2 infection.[67,68]

Altogether, our study defines the K18 hACE2 transgenic mouse as an important small animal model to evaluate SARS-CoV-2 pathogenicity and to assess protection efficacy of prophylactic (vaccines) and therapeutic (antivirals) approaches against SARS-CoV-2 infection with specific readouts such as morbidity, mortality, cytokine and chemokine storms, histopathology, and viral replication.

ACKNOWLEDGMENTS

We would like to thank all members of Texas Biomedical Research Institute for their efforts in keeping the institute fully operational during the COVID-19 pandemic, making this study possible. We would also like to thank the support of Texas Biomed donors, whose COVID-19 philanthropic donations made possible the realization of this study. We thank Dr. Abul Azad for his assistance with editing. Finally, we would also like to thank The Jackson Laboratory, especially Drs. Cat Lutz and Steve Rockwood, for providing us with K18 hACE2 transgenic mice to conduct this study; and the Texas Biomed IACUC and BSC committees and EHS for their attention to review our protocols in a time efficient manner to facilitate rapid sharing of our data with the scientific community. We would like to dedicate this manuscript to all COVID-19 victims and to all heroes battling this disease.

CONFLICT OF INTEREST

Authors declare not conflict of interest.

AUTHORS CONTRIBUTIONS

Planned, executed studies and data analyses (FSO, J-GP, PPT, OG, AA, AAG, AOF, SG, AGV, CY, KC, CH, VDLP, LMP , KJA, HMS, AS, JIG, AW, RNP, MG, JM, CC, SE, OHR, SDM, KNK, RE, SHU, XA, JT, LMS and JBT); Edited the manuscript (OG, CRAH, C-Christi, JLP, TA, RCJr, LDG, EJDJr, DK, and LSS); Wrote the manuscript (JT, LMS and JBT).

637 **Table 1. Histopathology evaluation of SARS-CoV-2 infected WT and K18 hACE2 transgenic C57BL/6**
638 **mice.** F: female. M: Male. When not indicated, observed in the majority of females and males.

	DAY 2		DAY 4	
GROUP	**Lung**	**Other**	**Lung**	**Other**
C57BL/6 WT	▪ Minimal or mild multifocal random areas of interstitial thickening with mixed mononuclear cells and neutrophils and minimal intra-alveolar hemorrhage (4 F). ▪ Rare vasculitis (1 F) ▪ Multiple yet minimal perivascular mononuclear cells, low neutrophil numbers. ▪ Rare or few bronchiolar syncytia. (2 F/2 M) ▪ Focal minimal aggregates of histiocytes. Focal accumulation of amorphous eosinophilic material in alveolar space (fibrin) (1M).	**Nasal cavity:** Minimal to mild neutrophil infiltration in (1 F/1 M). **Liver:** Minimal random multifocal aggregates of histiocytes, lymphocytes and few neutrophils. Rare necrotic hepatocytes within hepatic lobule (4 F/3 M) **Small and large intestine:** Small focal aggregates of lymphocytes and rare scattered neutrophils in lamina propria (Gut-associated lymphoid tissue, GALT). (2 F) **Kidney:** Focal small aggregate of neutrophils and histiocytes in interstitium of peri-renal adipose tissue, and medullary interstitium. Eosinophilic material in few glomeruli urinary spaces (1 M) **Heart:** Small lymphoid aggregates within adipose tissue surrounding artery (1 F)	▪ Minimal perivascular and interstitial involvement. ▪ Few neutrophils seen admixed with mononuclear inflammatory sites. ▪ Occasional alveolar epithelial type II cells in areas of alveolar wall septal inflammation (4 F/2 M) ▪ Rare vasculitis (1F) ▪ Few bronchiole syncytia (4 F/1 M).	**Nasal cavity:** In the majority, minimal or no changes. Large focal aggregate of lymphocytes and neutrophils in submucosa (1 F). **Liver:** Minimal to mild random multifocal aggregates of histiocytes, lymphocytes and few neutrophils. Rare necrotic hepatocytes within hepatic lobule (3 F/3 M) **Small and large intestine:** Multifocal minimal aggregates of lymphocytes within the lamina propria (GALT) (2 F/2 M).
K18 hACE2	▪ Mild or moderate mononuclear and neutrophilic inflammation admixed with necrotic cell debris. ▪ Predominant perivascular pattern expanding into alveolar septa. ▪ Mild to moderate alveolar histiocytosis. ▪ Mild alveolar epithelial cell type II hyperplasia. ▪ Bronchiolar syncytia ▪ Endothelial syncytia and vasculitis. ▪ Focal evidence of aspiration pneumonia.	**Nasal cavity:** Few neutrophils within submucosa. Some lymphocyte, rare neutrophils (1 F/2 M). **Liver:** Minimal multifocal small aggregates of lymphocytes, histiocytes, neutrophils in hepatic cords (4 F/2 M). **Small/Large intestine:** Focal large/small lymphoid aggregates (GALT) (2 F/2 M). Few neutrophils in lamina propria (1 M). **Kidney:** Few focal areas of interstitial lymphocytes in deep cortex (1 F). Regional cystic dilation of renal pelvis (1 M).	▪ 25% or less (4 F/2 M) or >25% (2 M) of lung with dense mild to moderate mixed inflammatory infiltrate (macrophages, neutrophils) (3 F). ▪ Regional consolidation mixed with necrotic debris. ▪ Occasional intra-alveolar and perivascular hemorrhage. ▪ Mild to moderate mixed mononuclear and neutrophilic inflammation. ▪ Predominant interstitial, intra-alveolar and perivascular patterns of mixed inflammation. ▪ Multifocal involvement of peribronchiolar, bronchiolar, and pleura in more severely affected areas. ▪ Mild to moderate histiocytosis.	**Nasal cavity:** Few foci of neutrophils, few lymphocytes (3 M). Low numbers of submucosal lymphocyte and plasma cell (1 M). **Liver:** Few focal aggregates of neutrophils, histiocytes, and lymphocytes (2 F/4 M). **Small and large intestine:** Focal small aggregate of lymphocytes or neutrophils in laminar propria (3 F/2 M). **Brain:** Multifocal perivascular hemorrhage (1 F). Multifocal perivascular lymphocytes, rare neutrophils, reactive microglial cells, neuronal necrosis and necrotic debris, vasculitis, inflammation extended to meninges (1M).

			▪ Mild pneumocyte type II hyperplasia. ▪ Frequent vasculitis and endothelial syncytia. ▪ Minimal intra-alveolar fibrin. Bronchiolar syncytia present. ▪ Regional perivascular edema admixed with mononuclear inflammation (1 M).	

CONTROLS: WT 57BL/6 and K18 hACE2 transgenic mock infected mice were assessed at the completion of the study, and showed no significant, or mild, microscopic lesions. Specifically, WT C57BL/6 mock infected mice has no significant lesions, with the exception of prominent lymphoid follicles within the lamina propria (GALT) and spleenic white pulp (1M), or small lymphocyte aggregates admixed with few neutrophils in the hepatic sinusoids (1F). K18 ACE2 transgenic mock infected mice had minor findings; two small focal perivascular aggregates of lymphocytes, few small lymphocyte aggregates, and focal osseous metaplasia within the pleura; few small aggregates of histiocytes and lymphocytes admixed with few neutrophils within hepatic sinusoids and occasionally in portal triads; prominent lymphoid follicles within gastrointestinal lamina propria (M); and macrophages within the splenic red pulp with minimal yellow intracytoplasmic pigment (1F).

REFERENCES

1 Hoffmann, M. *et al.* SARS-CoV-2 Cell Entry Depends on ACE2 and TMPRSS2 and Is Blocked by a Clinically Proven Protease Inhibitor. *Cell* **181**, 271-280 e278, doi:10.1016/j.cell.2020.02.052 (2020).

2 Lu, R. *et al.* Genomic characterisation and epidemiology of 2019 novel coronavirus: implications for virus origins and receptor binding. *Lancet* **395**, 565-574, doi:10.1016/S0140-6736(20)30251-8 (2020).

3 Walls, A. C. *et al.* Structure, Function, and Antigenicity of the SARS-CoV-2 Spike Glycoprotein. *Cell* **181**, 281-292 e286, doi:10.1016/j.cell.2020.02.058 (2020).

4 Yan, R. *et al.* Structural basis for the recognition of SARS-CoV-2 by full-length human ACE2. *Science* **367**, 1444-1448, doi:10.1126/science.abb2762 (2020).

5 Gheblawi, M. *et al.* Angiotensin-Converting Enzyme 2: SARS-CoV-2 Receptor and Regulator of the Renin-Angiotensin System: Celebrating the 20th Anniversary of the Discovery of ACE2. *Circ Res* **126**, 1456-1474, doi:10.1161/CIRCRESAHA.120.317015 (2020).

6 Zhou, F. *et al.* Clinical course and risk factors for mortality of adult inpatients with COVID-19 in Wuhan, China: a retrospective cohort study. *Lancet* **395**, 1054-1062, doi:10.1016/S0140-6736(20)30566-3 (2020).

7 Zhang, J. *et al.* Risk factors for disease severity, unimprovement, and mortality in COVID-19 patients in Wuhan, China. *Clin Microbiol Infect*, doi:10.1016/j.cmi.2020.04.012 (2020).

8 Li, X. *et al.* Risk factors for severity and mortality in adult COVID-19 inpatients in Wuhan. *J Allergy Clin Immunol*, doi:10.1016/j.jaci.2020.04.006 (2020).

9 Gattinoni, L. *et al.* Covid-19 Does Not Lead to a "Typical" Acute Respiratory Distress Syndrome. *Am J Respir Crit Care Med*, doi:10.1164/rccm.202003-0817LE (2020).

10 Gattinoni, L., Chiumello, D. & Rossi, S. COVID-19 pneumonia: ARDS or not? *Crit Care* **24**, 154, doi:10.1186/s13054-020-02880-z (2020).

11 McCray, P. B., Jr. *et al.* Lethal infection of K18-hACE2 mice infected with severe acute respiratory syndrome coronavirus. *J Virol* **81**, 813-821, doi:10.1128/JVI.02012-06 (2007).

12 Moreau, G. B., SK, Sturek, JM; Donla,n AN; Petri, WA Jr.; Mann, BJ. Evaluation of K18-hACE2 mice as a model of SARS-CoV-2 infection. https://www.biorxiv.org/content/10.1101/2020.06.26.171033v1. *BioRxiv*, doi:https://doi.org/10.1101/2020.06.26.171033 (2020).

13 Rathnasinghe, R. S., S; Amanat, F; Gillespie, VL; Krammer, F; Garcia-Sastre, A; Coughlan, L; Schotsaert, M; Uccellini M. Comparison of Transgenic and Adenovirus hACE2 Mouse Models for SARS-CoV-2 Infection. https://www.biorxiv.org/content/10.1101/2020.07.06.190066v1. *BioRxiv* (2020).

14 Jiang, R. D. *et al.* Pathogenesis of SARS-CoV-2 in Transgenic Mice Expressing Human Angiotensin-Converting Enzyme 2. *Cell* **182**, 50-58 e58, doi:10.1016/j.cell.2020.05.027 (2020).

15 Sun, S.-H., Chen, Q., Gu, H.-J., Yang, G., Wang, Y.-X., Huang, X.-Y., Liu, S.-S., Zhang, N.-N., Li, X.-F., Xiong, R., Guo, Y., Deng, Y.-Q., Huang, W.-J., Liu, Q., Liu, Q.-M., Shen, Y.-L.,

680 Zhou, Y., Yang, X., Zhao, T.-Y., Fan, C.-F., Zhou, Y.-S., Qin, C.-F., Wang, Y.-C. A mouse model
681 of SARS-CoV-2 infection and pathogenesis. *Cell Host Microbe*, https://doi.org/10.1016/j.chom.
682 2020.1005.1020., doi:https://doi.org/10.1016/j.chom.2020.05.020. (2020).
683 16 Bao, L. *et al.* The pathogenicity of SARS-CoV-2 in hACE2 transgenic mice. *Nature*,
684 doi:10.1038/s41586-020-2312-y (2020).
685 17 Hassan, A. O. *et al.* A SARS-CoV-2 Infection Model in Mice Demonstrates Protection by
686 Neutralizing Antibodies. *Cell*, doi:10.1016/j.cell.2020.06.011 (2020).
687 18 Israelow, B. *et al.* Mouse model of SARS-CoV-2 reveals inflammatory role of type I
688 interferon signaling. *bioRxiv*, doi:10.1101/2020.05.27.118893 (2020).
689 19 Sun, J. *et al.* Generation of a Broadly Useful Model for COVID-19 Pathogenesis,
690 Vaccination, and Treatment. *Cell*, doi:10.1016/j.cell.2020.06.010 (2020).
691 20 Kaushal, D. *et al.* Mucosal vaccination with attenuated Mycobacterium tuberculosis
692 induces strong central memory responses and protects against tuberculosis. *Nat. Commun* **6**,
693 8533, doi:ncomms9533 [pii];10.1038/ncomms9533 [doi] (2015).
694 21 Foreman, T. W. *et al.* CD4+ T-cell-independent mechanisms suppress reactivation of
695 latent tuberculosis in a macaque model of HIV coinfection. *Proc Natl Acad Sci U S A* **113**,
696 E5636-5644, doi:10.1073/pnas.1611987113 (2016).
697 22 Coperchini, F., Chiovato, L., Croce, L., Magri, F. & Rotondi, M. The cytokine storm in
698 COVID-19: An overview of the involvement of the chemokine/chemokine-receptor system.
699 *Cytokine Growth Factor Rev* **53**, 25-32, doi:10.1016/j.cytogfr.2020.05.003 (2020).
700 23 Song, P., Li, W., Xie, J., Hou, Y. & You, C. Cytokine storm induced by SARS-CoV-2. *Clin*
701 *Chim Acta* **509**, 280-287, doi:10.1016/j.cca.2020.06.017 (2020).
702 24 Costela-Ruiz, V. J., Illescas-Montes, R., Puerta-Puerta, J. M., Ruiz, C. & Melguizo-
703 Rodriguez, L. SARS-CoV-2 infection: The role of cytokines in COVID-19 disease. *Cytokine*
704 *Growth Factor Rev*, doi:10.1016/j.cytogfr.2020.06.001 (2020).

25 Ye, Q., Wang, B. & Mao, J. The pathogenesis and treatment of the `Cytokine Storm' in COVID-19. *J Infect* **80**, 607-613, doi:10.1016/j.jinf.2020.03.037 (2020).

26 Zhang, X. *et al.* Viral and host factors related to the clinical outcome of COVID-19. *Nature*, doi:10.1038/s41586-020-2355-0 (2020).

27 Ong, E. Z. *et al.* A Dynamic Immune Response Shapes COVID-19 Progression. *Cell Host Microbe* **27**, 879-882 e872, doi:10.1016/j.chom.2020.03.021 (2020).

28 Speirs, I. T., NC. Sex differences in hippocampal cytokines after systemic immune challenge - https://www.biorxiv.org/content/10.1101/378257v1. *BioRxiv* (2020).

29 Posilico, C. S., IC; Tronson, NC. Sex differences in the hippocampal cytokine response following systemic lipopolysaccharide. *Brain, Behavior, and Immunity* **66**, e40, doi:https://doi.org/10.1016/j.bbi.2017.07.145 (2017).

30 Toietta, G. *et al.* Reduced inflammation and improved airway expression using helper-dependent adenoviral vectors with a K18 promoter. *Mol Ther* **7**, 649-658, doi:10.1016/s1525-0016(03)00059-5 (2003).

31 Laboratory, T. J. *B6.Cg-Tg(K18-ACE2)2Prlmn/J - K18 hACE2 mouse - https://www.jax.org/strain/034860* (2020).

32 Li; Qi Lv; Jing Xue; Shuran Gong; Mingya Liu; Guanpeng Wang; Shunyi Wang; Linna Zhao; Peipei Liu; Li Zhao; Fei Ye; Huijuan Wang; Weimin Zhou; Na Zhu; Wei Zhen; Xiaojuan Zhang; Zhiqi Song; Li Guo; Lan Chen; Conghui Wang; Ying Wang; Xinming Wang; Yan Xiao; Qiangming Sun; Hongqi Liu; Fanli Zhu; Chunxia Ma; Lingmei Yan; Mengli Yan; Jun Han; Wenbo Xu; Wenjie Tan; Xiaozhong Peng; Qi Jin; Guizhen Wu; Chuan Qin, L. B. W. D. B. H. H. G. L. R. Q. W. P. Y. Y. X. J. L. F. Q. Y. Q. W. W. F. The Pathogenicity of 2019 Novel Coronavirus in hACE2 Transgenic Mice. *BioRxiv* **https://doi.org/10.1101/2020.02.07.939389** (2020).

33 Lofgren, E., Fefferman, N. H., Naumov, Y. N., Gorski, J. & Naumova, E. N. Influenza seasonality: underlying causes and modeling theories. *J Virol* **81**, 5429-5436, doi:10.1128/JVI.01680-06 (2007).

731 34 Tisoncik, J. R. *et al.* Into the eye of the cytokine storm. *Microbiol Mol Biol Rev* **76**, 16-32,
732 doi:10.1128/MMBR.05015-11 (2012).
733 35 Yuen, K. Y. & Wong, S. S. Human infection by avian influenza A H5N1. *Hong Kong Med*
734 *J* **11**, 189-199 (2005).
735 36 Huang, K. J. *et al.* An interferon-gamma-related cytokine storm in SARS patients. *J Med*
736 *Virol* **75**, 185-194, doi:10.1002/jmv.20255 (2005).
737 37 Cameron, M. J. *et al.* Interferon-mediated immunopathological events are associated
738 with atypical innate and adaptive immune responses in patients with severe acute respiratory
739 syndrome. *J Virol* **81**, 8692-8706, doi:10.1128/JVI.00527-07 (2007).
740 38 Moyron-Quiroz, J. E. *et al.* Role of inducible bronchus associated lymphoid tissue
741 (iBALT) in respiratory immunity. *Nat Med* **10**, 927-934, doi:10.1038/nm1091 (2004).
742 39 Park, W. Y. *et al.* Cytokine balance in the lungs of patients with acute respiratory distress
743 syndrome. *Am J Respir Crit Care Med* **164**, 1896-1903, doi:10.1164/ajrccm.164.10.2104013
744 (2001).
745 40 Sun, L. *et al.* New concepts of IL-10-induced lung fibrosis: fibrocyte recruitment and M2
746 activation in a CCL2/CCR2 axis. *Am J Physiol Lung Cell Mol Physiol* **300**, L341-353,
747 doi:10.1152/ajplung.00122.2010 (2011).
748 41 Tanaka, T. & Kishimoto, T. The biology and medical implications of interleukin-6. *Cancer*
749 *Immunol Res* **2**, 288-294, doi:10.1158/2326-6066.CIR-14-0022 (2014).
750 42 Antczak, A. *et al.* Analysis of changes in expression of IL-4/IL-13/STAT6 pathway and
751 correlation with the selected clinical parameters in patients with atopic asthma. *Int J*
752 *Immunopathol Pharmacol* **29**, 195-204, doi:10.1177/0394632015623794 (2016).
753 43 Junttila, I. S. Tuning the Cytokine Responses: An Update on Interleukin (IL)-4 and IL-13
754 Receptor Complexes. *Front Immunol* **9**, 888, doi:10.3389/fimmu.2018.00888 (2018).
755 44 Chen, Z. *et al.* IL-6, IL-10 and IL-13 are associated with pathogenesis in children with
756 Enterovirus 71 infection. *Int J Clin Exp Med* **7**, 2718-2723 (2014).

757 45 Kasashima, S. *et al.* Upregulated interleukins (IL-6, IL-10, and IL-13) in immunoglobulin
758 G4-related aortic aneurysm patients. *J Vasc Surg* **67**, 1248-1262, doi:10.1016/j.jvs.2016.12.140
759 (2018).
760 46 Kenney, A. D. *et al.* IFITM3 protects the heart during influenza virus infection. *Proc Natl*
761 *Acad Sci U S A* **116**, 18607-18612, doi:10.1073/pnas.1900784116 (2019).
762 47 Biernacki, K., Prat, A., Blain, M. & Antel, J. P. Regulation of Th1 and Th2 lymphocyte
763 migration by human adult brain endothelial cells. *J Neuropathol Exp Neurol* **60**, 1127-1136,
764 doi:10.1093/jnen/60.12.1127 (2001).
765 48 Gadani, S. P., Cronk, J. C., Norris, G. T. & Kipnis, J. IL-4 in the brain: a cytokine to
766 remember. *J Immunol* **189**, 4213-4219, doi:10.4049/jimmunol.1202246 (2012).
767 49 de Aquino, M. T. *et al.* IL-27 limits central nervous system viral clearance by promoting
768 IL-10 and enhances demyelination. *J Immunol* **193**, 285-294, doi:10.4049/jimmunol.1400058
769 (2014).
770 50 Yoshida, H. & Hunter, C. A. The immunobiology of interleukin-27. *Annu Rev Immunol*
771 **33**, 417-443, doi:10.1146/annurev-immunol-032414-112134 (2015).
772 51 Strle, K. *et al.* Interleukin-10 in the brain. *Crit Rev Immunol* **21**, 427-449 (2001).
773 52 Kawanokuchi, j. T., H; Sonobe, Y; Mizuno, T; Suzumura, A. Interleukin-27 promotes
774 inflammatory and neuroprotective responses in microglia. *Clinical & Experimental*
775 *Neuroimmunology* **4**, 36-45 (2013).
776 53 Deczkowska, A., Baruch, K. & Schwartz, M. Type I/II Interferon Balance in the
777 Regulation of Brain Physiology and Pathology. *Trends Immunol* **37**, 181-192,
778 doi:10.1016/j.it.2016.01.006 (2016).
779 54 Kuba, K. *et al.* A crucial role of angiotensin converting enzyme 2 (ACE2) in SARS
780 coronavirus-induced lung injury. *Nat Med* **11**, 875-879, doi:10.1038/nm1267 (2005).
781 55 Wood, H. New insights into the neurological effects of COVID-19. *Nat Rev Neurol*,
782 doi:10.1038/s41582-020-0386-7 (2020).

56 Lan, J. *et al.* Structure of the SARS-CoV-2 spike receptor-binding domain bound to the ACE2 receptor. *Nature*, doi:10.1038/s41586-020-2180-5 (2020).

57 Wan, Y., Shang, J., Graham, R., Baric, R. S. & Li, F. Receptor Recognition by the Novel Coronavirus from Wuhan: an Analysis Based on Decade-Long Structural Studies of SARS Coronavirus. *J Virol* **94**, doi:10.1128/JVI.00127-20 (2020).

58 Wang, Q. *et al.* Structural and Functional Basis of SARS-CoV-2 Entry by Using Human ACE2. *Cell*, doi:10.1016/j.cell.2020.03.045 (2020).

59 Shang, J. *et al.* Structural basis of receptor recognition by SARS-CoV-2. *Nature* **581**, 221-224, doi:10.1038/s41586-020-2179-y (2020).

60 Yu, J. *et al.* DNA vaccine protection against SARS-CoV-2 in rhesus macaques. *Science*, doi:10.1126/science.abc6284 (2020).

61 Chandrashekar, A. *et al.* SARS-CoV-2 infection protects against rechallenge in rhesus macaques. *Science*, doi:10.1126/science.abc4776 (2020).

62 Singh, D. G., SR; Singh, B; Cole, J; 1,2,Alfson KJ; Clemmons, E; ,Gazi, M; Gonzalez, O; Escobedo, R; Lee, T-H; Chatterjee, A; Goez-Gazi, Y; Sharan, R; Thippeshappa, R; Gough, M; Alvarez, C; Blakley, A; Ferdin, J; Bartley, C; Staples, H; Parodi, P; Callery, J; Mannino, A; Klaffke, B; Escareno, P; PlattII, RN; Hodara, V; Scordo, JM; Oyejide, A; Ajithdoss DK; Copin, R; Baum, A; Kyratsous, C; Alvarez, X; Rosas, B; Ahmed, M; Goodroe, A; Dutton, J; Hall-Ursone, S; Frost, PA; Voges, AK; Ross, CN; Sayers, K; Chen, C; Hallam, C; Khader, SA; Mitreva, M; Anderson. TJC; Martinez-Sobrido, L; Patterson, JL; Turner, J; Torrelles, JB; Dick Jr, EJ; Brasky, K; Schlesinger, LS; Giavedoni, LD; Carrion Jr, R; Kaushal, D. SARS-CoV-2 infection leads to acute infection with dynamic cellular and inflammatory flux in the lung that varies across nonhuman primate species - https://www.biorxiv.org/content/10.1101/2020.06.05.136481v1. *BioRxiv* (2020).

63 Woolsey, C. *et al.* Establishment of an African green monkey model for COVID-19. *bioRxiv*, doi:10.1101/2020.05.17.100289 (2020).

64 Boudewijns, R. T., HJ; Kaptein, SFJ; Li, R; Vergote, V; Seldeslachts, L; De Keyzer, C; Sharma, S; Jansen, S; Van Weyenbergh, J; Ma, J; Marten,s E; et al. . STAT2 signaling as double-edged sword restricting viral dissemination but driving severe pneumonia in SARS-CoV-2 infected hamsters. https://doi.org/10.1101/2020.04.23.056838. *bioRxiv*, doi:https://doi.org/10.1101/2020.04.23.056838 (2020).

65 Chan, J. F. *et al.* Simulation of the clinical and pathological manifestations of Coronavirus Disease 2019 (COVID-19) in golden Syrian hamster model: implications for disease pathogenesis and transmissibility. *Clin Infect Dis*, doi:10.1093/cid/ciaa325 (2020).

66 Sia, S. Y., L-M; Chin AWH; Fung, K; Poon, LLM; Nicholls, JM; Peiris, M; Yen H-L. *Pathogenesis and transmission of SARS-CoV-2 virus in golden Syrian hamsters - DOI: 10.21203/rs.3.rs-20774/v1*, 2020).

67 Arimori, Y. *et al.* Type I interferon limits influenza virus-induced acute lung injury by regulation of excessive inflammation in mice. *Antiviral Res* **99**, 230-237, doi:10.1016/j.antiviral.2013.05.007 (2013).

68 Shepardson, K. M. *et al.* IFNAR2 Is Required for Anti-influenza Immunity and Alters Susceptibility to Post-influenza Bacterial Superinfections. *Front Immunol* **9**, 2589, doi:10.3389/fimmu.2018.02589 (2018).

FIGURE LEGENDS

Figure 1. Infection of K18 hACE2 transgenic and WT C57BL/6 mice with SARS-CoV-2. K18 hACE2 transgenic and WT C57BL/6 female and male mice were mock-infected (N=3/group) or infected i.n. (N=4/group) with 1 x 10^5 PFU of SARS-CoV-2. Body weight (**A**) and survival (**B**) were evaluated at the indicated DPI. Mice that loss more than 25% of their initial body weight were humanely euthanized. Error bars represent standard deviations (SD) of the mean for each group of mice. (**C-E**) K18 transgenic hACE2 and WT C57BL/6 male (N=3) and female (N=3) mice were similarly infected and sacrificed at 2 and 4 DPI and viral titers in different organs (nasal turbinate, trachea, lung, brain, heart, kidney, liver, spleen, small intestine, and large intestine) were determined by plaque assay (PFU/ml). Data from virus containing organs and/or tissue samples are shown: nasal turbinates (**C**), lungs (**D**) and brain (**E**). Symbols represent data from individual mouse, and bars the geometric means of viral titers. ND, not detected. Dotted lines indicate the limit of detection, LOD (10^2 PFU/ml). DPI: Days post-infection.

Figure 2. SARS-CoV-2 infected K18 hACE2 transgenic mice show a marked chemokine storm in selected tissues. (**A**) Lung, (**B**) spleen and (**C**) brain. Student's t-test C57BL/6 *vs.* K18 hACE2 *$p< 0.05; **$p<0.005; ***$p<0.0005; 2-WAY ANOVA C57BL/6 or K18 hACE2 transgenic mice over time, §p< 0.05; §§p<0.005; §§§p<0.0005, N= 8 (per time-point studied, except mock N=3). DPI: Days post-infection.

Figure 3. **SARS-CoV-2 infected K18 hACE2 transgenic mice show a marked cytokine storm in selected tissues.** (**A**) Lungs, (**B**) spleen and (**C**) brain. Student's t-test C57BL/6 *vs.* K18 hACE2 *$p< 0.05; **$p<0.005; ***$p<0.0005; 2-WAY ANOVA C57BL/6 or K18 hACE2 transgenic mice over time, §p< 0.05; §§p<0.005; §§§p<0.0005, N= 8 (per time-point studied, except mock N=2). DPI: Days post-infection.

Figure 4. SARS-CoV-2 infected K18 hACE2 transgenic mice reveal differentiated clusters of chemokine and cytokine correlations with clinical symptoms progression. Hierarchically clustered Pearson correlations of measurements in (**A**) lung, (**B**) spleen and (**C**) brain of SARS-CoV-2 infected K18 hACE2 transgenic mice. Positive correlation (Red = 1) and negative correlations (Blue = -1), with clusters (Black outlined boxes with cluster number). Non-significant values ($p > 0.05$ measured by Pearson's correlation t-test) were left blank. DPI: Days post-infection. MIP-2/CXCL2; MCP-1/CCL2; MIP-1α/CCL3; MIP-1β/CCL4; RANTES/CCL5; IP-10/CXCL10.

Figure 5. K18 hACE2 transgenic mice develop rhinitis, pneumonia with associated pulmonary inflammation after infection with SARS-CoV-2. (A-D and **I-L) WT C57BL/6 mice**. Minimal mononuclear and neutrophilic interstitial pneumonia in WT lung at 2-DPI (**A, B bracket**). By 4-DPI (**5C, D**) minimal alveolar histiocytosis (**D, asterisk**) pneumocyte type II cells (**D, arrowheads**), perivascular mononuclear inflammation (**D, bracket**) and rhinitis with low numbers of neutrophils (**K, arrowhead**) were variably observed. Lymphocyte aggregates in the lamina propria of the small intestine (**I, asterisk**). Mixed mononuclear inflammation with individual hepatocellular necrosis (**J, arrowhead**). Brain from WT 4-DPI was normal (**L**). **(E-H** and **M-P) K18 hACE2 transgenic mice**. Interstitial pneumonia (**E, F**) associated with alveolar histiocytosis admixed neutrophils and lymphocytes (**F, asterisks**), mild type II pneumocyte hyperplasia (**F, arrowhead**), bronchiolar syncytia (**F, arrow**), endothelial cells hyperplasia and vasculitis (**F, bracket**) by 2-DPI. Gut associated lymphoid tissue (GALT) with prominent germinal centers was observed (**M, asterisk**). Liver inflammation with variable amounts of individual hepatocellular necrosis (**N, arrowhead**). Greater lung involvement indicative of pneumonia (**G**), with inflammatory cellular accumulations and hemorrhage in alveolar spaces (**H, asterisk**) and interstitium (**H, bracket**), intra-alveolar fibrin admixed cellular debris (**H, arrow**), vasculitis (**H, bracket**), edema (**H, arrowhead**) by 4-DPI. Neutrophilic rhinitis observed at 4-DPI (**O, bracket**).

Mild meningoencephalitis with vasculitis (**P, arrowhead**). Scale bars left images, 1 mm. Scale bars right images, 50 μm. DPI: Days post-infection.

Figure 6. IHC examination of tissue from K18 hACE2 transgenic and WT C57BL/6 mice infected with SARS-CoV-2. (**A**) WT and K18 hACE2 transgenic C57BL/6 mice nasal turbinate (top, at 2-DPI), lung tissue (middle, at 2-DI) and brain (bottom, at 4-DPI) stained with an antibody against SARS-CoV-2 NP (red) or with antibody recognizing hACE2 receptor (red). (**B**) Infected choroid plexus in the brains of SARS-CoV-2-infected K18 hACE2 transgenic mice at 4-DPI. Left panel show that the hACE2 receptor (red) is highly expressed in the choroid plexus (all nuclei shown in aqua-blue). Right panel shows that some cells in the choroid plexus are infected with SARS-CoV-2 as these are positive to a SARS-CoV-2 NP (in red).

911 **SUPPLEMENTAL MATERIAL**

912 **Supplemental Figure legends**

913 **Figure S1. Infection of K18 hACE2 transgenic and WT C57BL/6 mice with SARS-CoV-2.**
914 Female and male K18 hACE2 transgenic and WT C57BL/6 mice were mock-infected (N=3/group)
915 or infected (N=4/group) i.n. with 1 x 10^5 PFU of SARS-CoV-2. Body weight (**A, B**) and survival (**C,**
916 **D**) were evaluated at the indicated DPI. Mice that loss more than 25% of their initial body weight
917 were humanely euthanized. Error bars represent standard deviations (SD) of the mean for each
918 group of mice. DPI: Days post-infection.

919

920 **Figure S2. Viral loads in male and female K18 hACE2 transgenic and WT C57BL/6 mice**
921 **infected with SARS-CoV-2.** K18 hACE2 transgenic and WT C57BL/6 male (N=4/group) and
922 female (N=4/group) mice were infected as in Figure S1 and sacrificed at 2- and 4-DPI and viral
923 titers in different organs (nasal turbinate, trachea, lung, brain, heart, kidney, liver, spleen, small
924 intestine, and large intestine) were determined by plaque assay (PFU/ml). Only data from virus
925 containing organs and/or tissue samples are shown: nasal turbinate (**A**), lungs (**B**) and brain (**C**).
926 Symbols represent data from individual mouse, and bars the geometric means of viral titers. @,
927 virus not detected in one mouse; &, virus not detected in two mice; #, virus not detected in three
928 mice; ND, not detected. Dotted black lines indicate the limit of detection (10^2 PFU/ml). DPI: Days
929 post-infection.

930

931 **Figure S3. Chemokine profile in selected tissues from SARS-CoV-2 infected K18 hACE2**
932 **transgenic mice.** (**A**) Nasal turbinates and (**B**) Trachea. Student's *t*-test C57BL/6 *vs.* K18 hACE2
933 **p*< 0.05; ***p*<0.005; ****p*<0.0005; 2-WAY ANOVA C57BL/6 or K18 hACE2 transgenic mice over
934 time, §p< 0.05; §§p<0.005; §§§p<0.0005, N= 8 (per time-point studied, except mock N=2). DPI:
935 Days post-infection.

Figure S4. Cytokine profile in selected tissues from SARS-CoV-2 infected K18 hACE2 transgenic mice. (**A**) Nasal turbinates and (**B**) Trachea. Student's t-test C57BL/6 *vs.* K18 transgenic hACE2 *p< 0.05; **p<0.005; ***p<0.0005; 2-WAY ANOVA C57BL/6 or K18 hACE2 transgenic mice over time, §p< 0.05; §§p<0.005; §§§p<0.0005, N= 8 (per time-point studied, except mock N=2). DPI: Days post-infection.

Figure S5. Chemokine and cytokine profile in selected tissues from SARS-CoV-2 infected K18 hACE2 transgenic mice by sex. Chemokines and cytokine differences in the (**A**) lung and (**B**) brain in K18 hACE2 transgenic and WT C57BL/6 male and female mice. Student's t-test C57BL/6 *vs.* K18 hACE2 *p< 0.05; **p<0.005; ***p<0.0005; 2-WAY ANOVA C57BL/6 or K18 hACE2 transgenic mice over time, §p< 0.05; §§p<0.005; §§§p<0.0005, N= 4/group/sex (per time-point studied, except mock N=2). DPI: Days post-infection.

Figure S6. SARS-CoV-2 infected K18 hACE2 transgenic mice reveal differentiated clusters of chemokine and cytokine correlations with clinical symptoms progression. Hierarchically clustered Pearson correlations of measurements in (**A**) nasal turbinate and (**B**) trachea of SARS-CoV-2 infected K18 hACE2 transgenic mice (Left: 2-DPI, Right: 4-DPI). Positive correlation (Red = 1) and negative correlations (Blue = -1), with clusters (Black outlined boxes with cluster number). Non-significant values ($p > 0.05$ measured by Pearson's correlation t-test) left blank. DPI: Days post-infection. MIP-2/CXCL2; MCP-1/CCL2; MIP-1α/CCL3; MIP-1β/CCL4; RANTES/CCL5; IP-10/CXCL10.

Figure S7. **Immune response of SARS-CoV-2 infected K18 hACE2 transgenic mice is dependent on mouse sex.** Hierarchically clustered Pearson correlations of measurements in lung at (**A**) 2- and (**B**) 4-DPI and brain at (**C**) 2- and (**D**) 4-DPI of SARS-CoV-2 infected K18 hACE2

961 transgenic mice (Left: Males, Right: Females). Positive correlation (Red = 1) and negative
962 correlations (Blue = -1), with clusters (Black outlined boxes with cluster number). Non-significant
963 values ($p > 0.05$ measured by Pearson's correlation t-test) left blank. DPI: Days post-infection.
964 MIP-2/CXCL2; MCP-1/CCL2; MIP-1α/CCL3; MIP-1β/CCL4; RANTES/CCL5; IP-10/CXCL10.
965
966
967

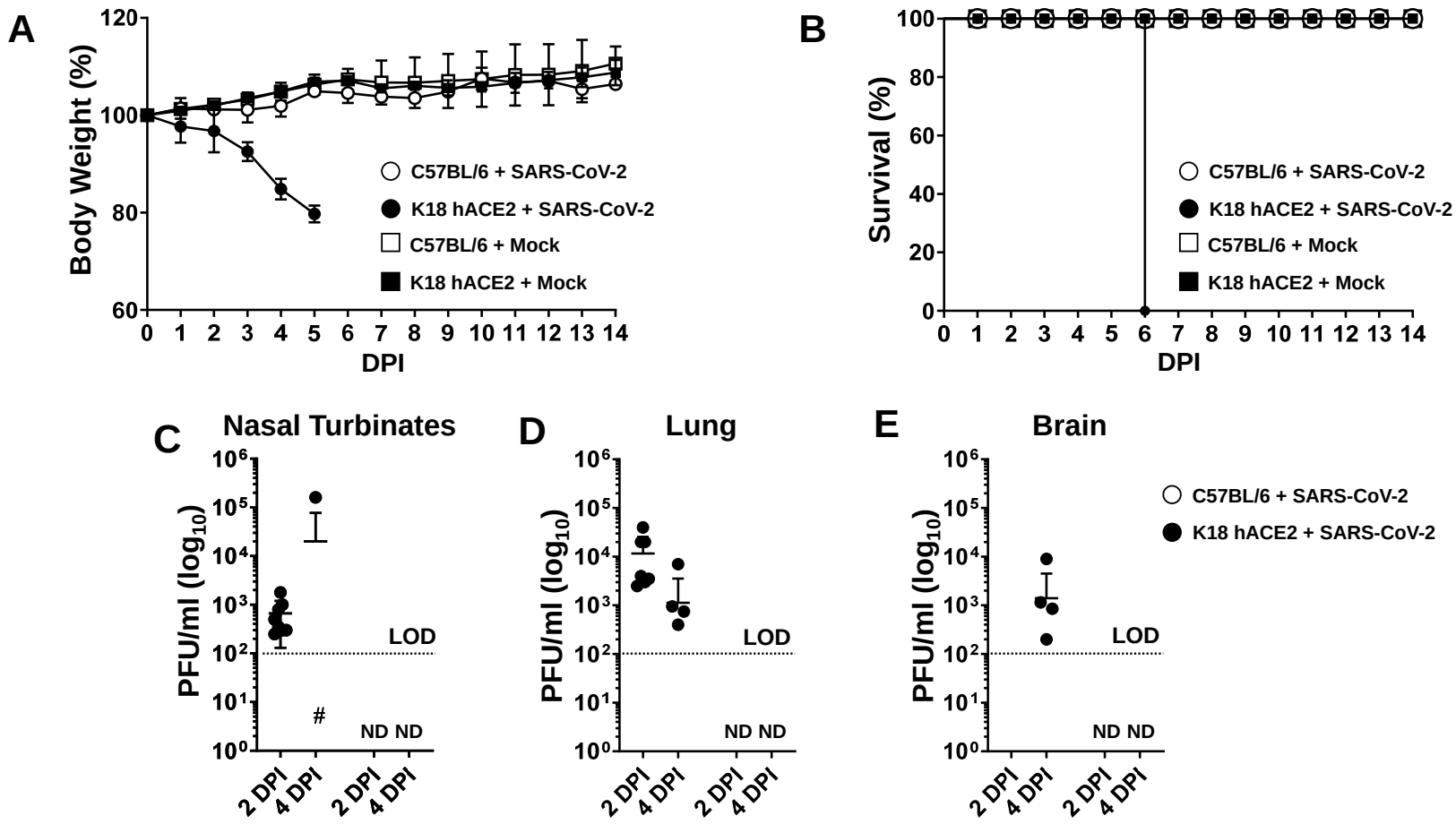

Figure 1. Infection of K18 hACE2 transgenic and WT C57BL/6 mice with SARS-CoV-2. K18 hACE2 transgenic and WT C57BL/6 female and male mice were mock-infected (N=3/group) or infected i.n. (N=4/group) with 1 x 10^5 PFU of SARS-CoV-2. Body weight (**A**) and survival (**B**) were evaluated at the indicated DPI. Mice that loss more than 25% of their initial body weight were humanely euthanized. Error bars represent standard deviations (SD) of the mean for each group of mice. (**C-E**) K18 transgenic hACE2 and WT C57BL/6 male (N=3) and female (N=3) mice were similarly infected and sacrificed at 2 and 4 DPI and viral titers in different organs (nasal turbinate, trachea, lung, brain, heart, kidney, liver, spleen, small intestine, and large intestine) were determined by plaque assay (PFU/ml). Data from virus containing organs and/or tissue samples are shown: nasal turbinates (**C**), lungs (**D**) and brain (**E**). Symbols represent data from individual mouse, and bars the geometric means of viral titers. ND, not detected. Dotted lines indicate the limit of detection, LOD (10^2 PFU/ml). DPI: Days post-infection.

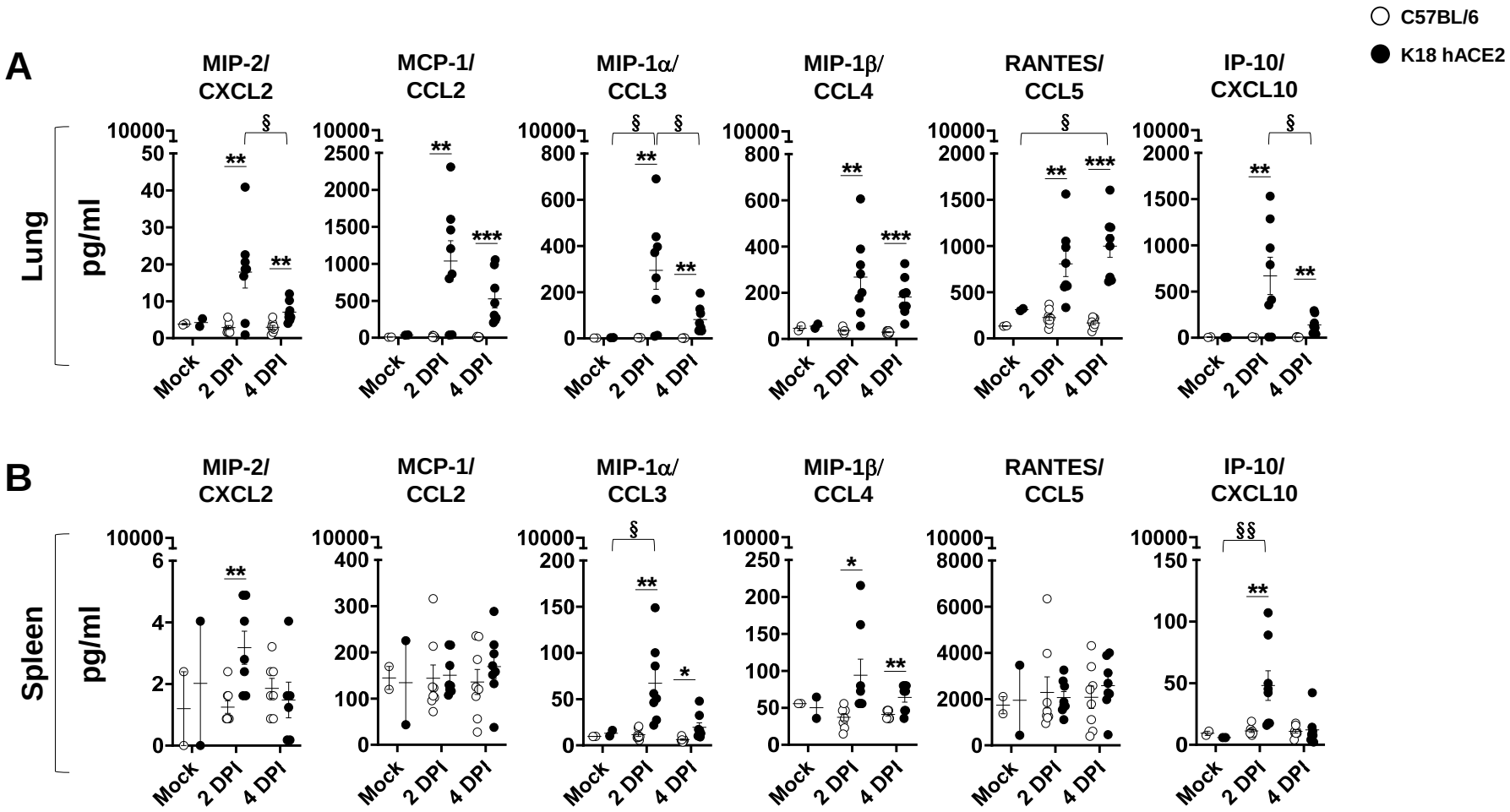

Figure 2. SARS-CoV-2 infected K18 hACE2 transgenic mice show a marked chemokine storm in selected tissues. (**A**) Lung, (**B**) spleen and (**C**) brain. Student's t-test C57BL/6 *vs.* K18 hACE2 *$p< 0.05$; **$p<0.005$; ***$p<0.0005$; 2-WAY ANOVA C57BL/6 or K18 hACE2 transgenic mice over time, §p< 0.05; §§p<0.005; §§§p<0.0005, N= 8 (per time-point studied, except mock N=3). DPI: Days post-infection.

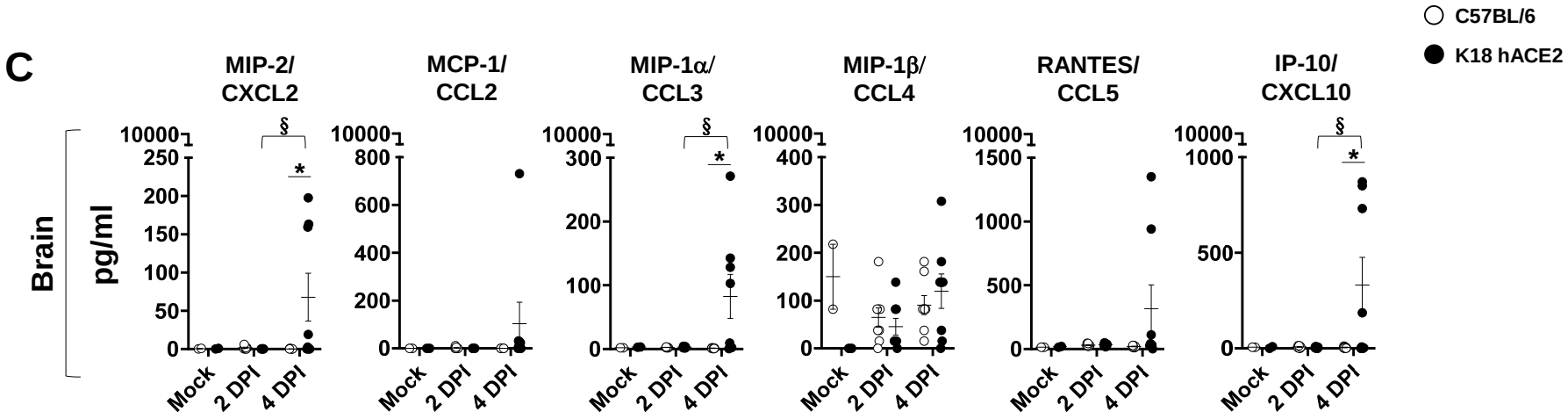

Figure 2. (Continuation).

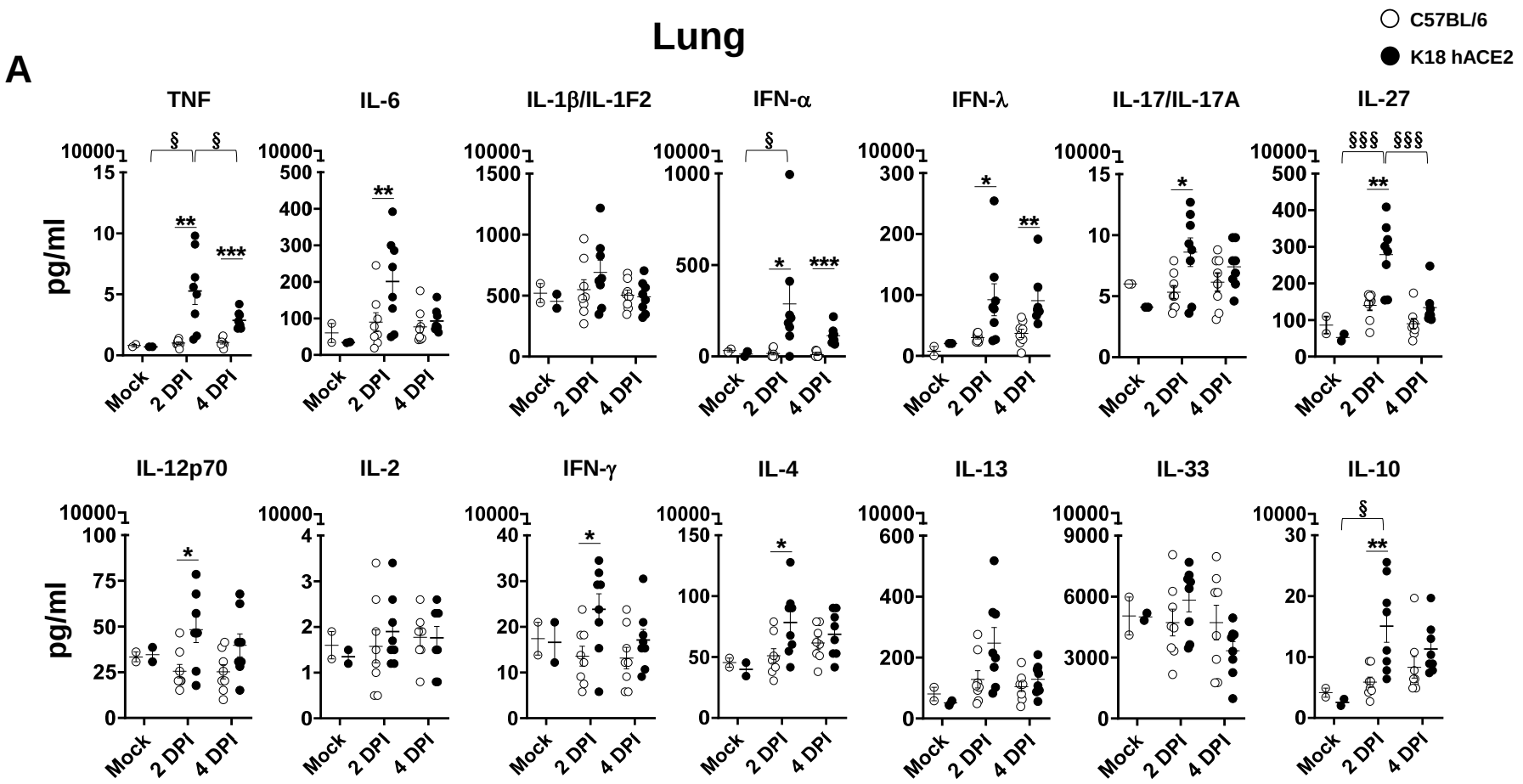

Figure 3. **SARS-CoV-2 infected K18 hACE2 transgenic mice show a marked cytokine storm in selected tissues.** (**A**) Lungs, (**B**) spleen and (**C**) brain. Student's t-test C57BL/6 *vs.* K18 hACE2 *$p< 0.05$; **$p<0.005$; ***$p<0.0005$; 2-WAY ANOVA C57BL/6 or K18 hACE2 transgenic mice over time, §p< 0.05; §§p<0.005; §§§p<0.0005, N= 8 (per time-point studied, except mock N=2). DPI: Days post-infection.

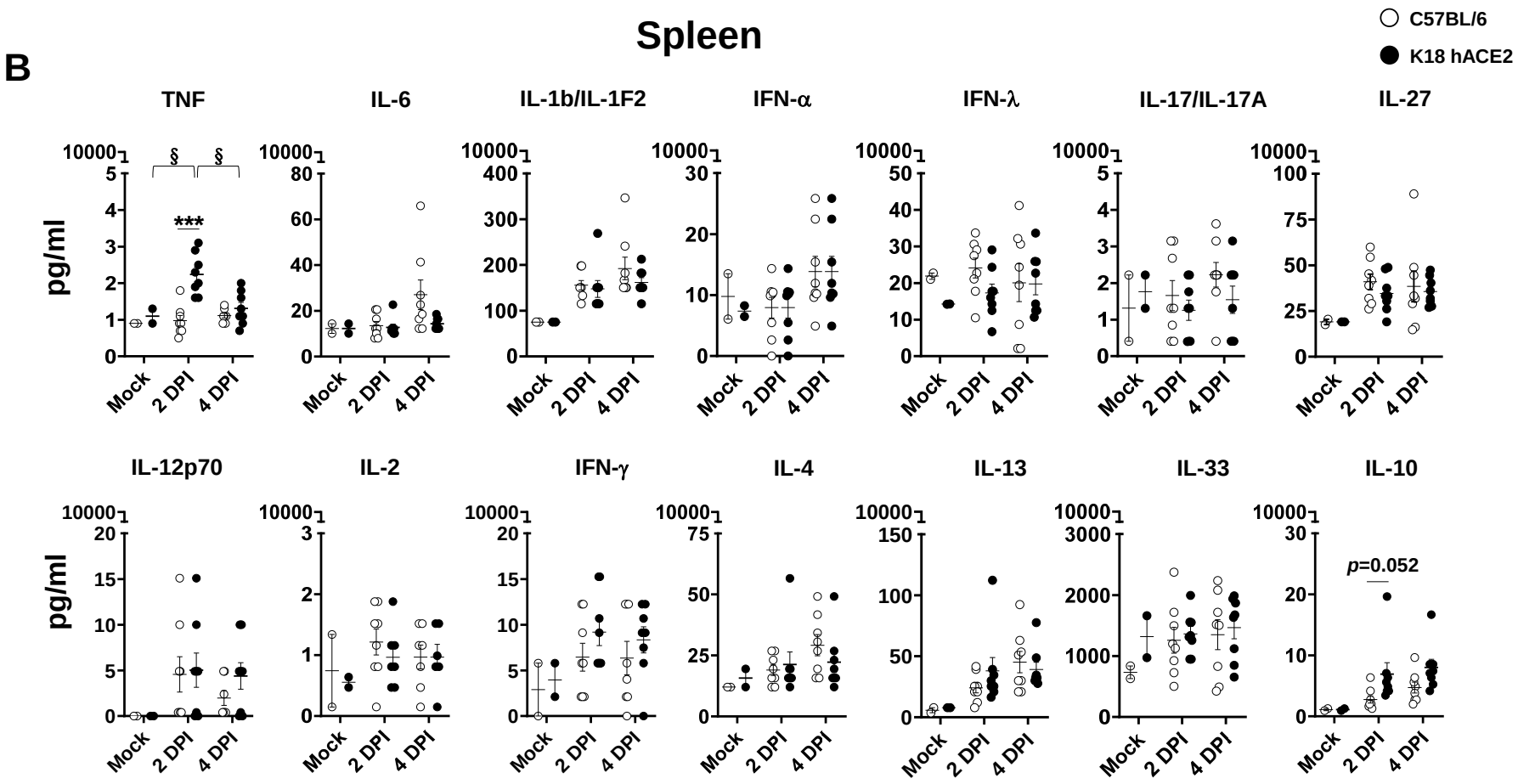

Figure 3. (Continuation).

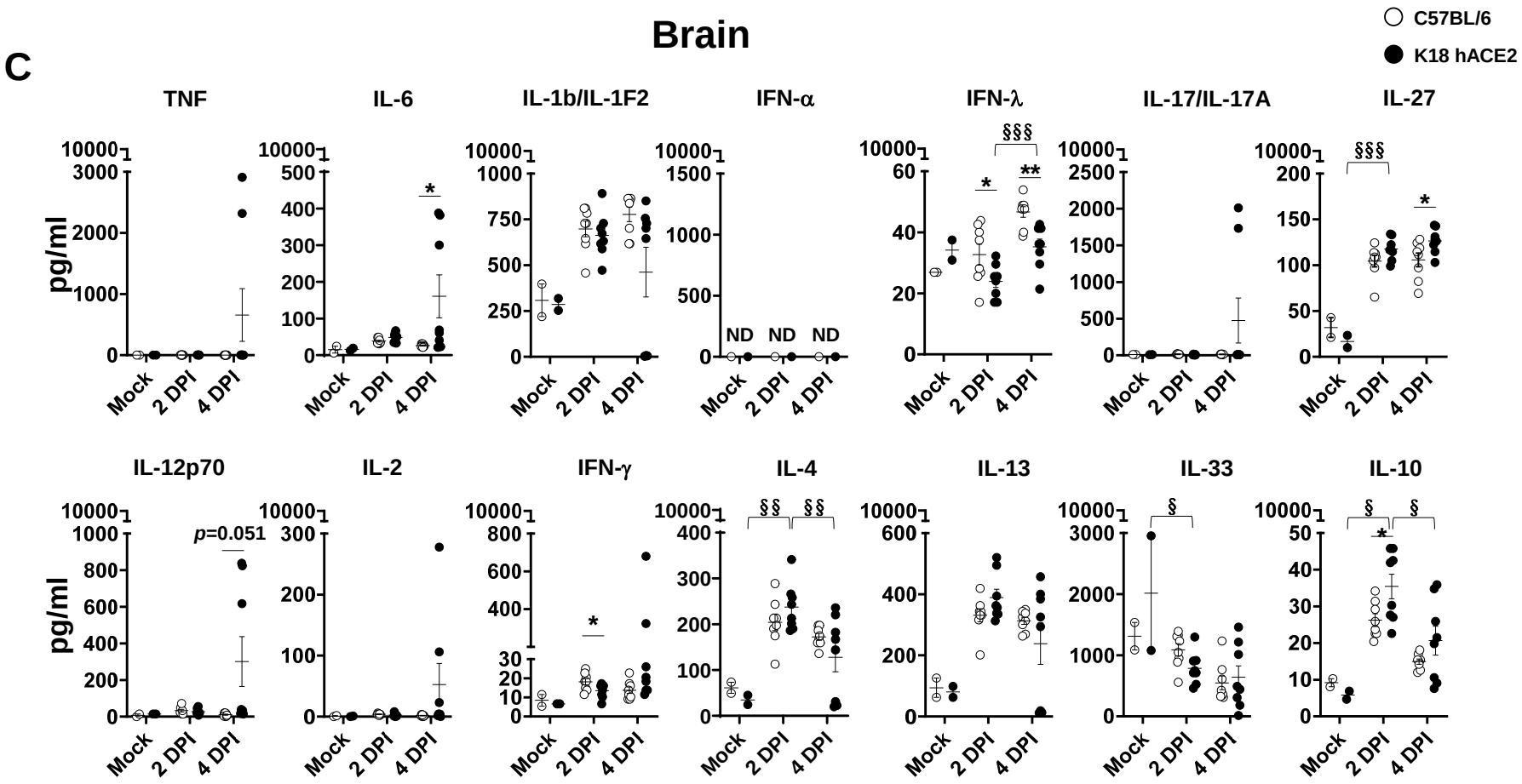

Figure 3. (Continuation).

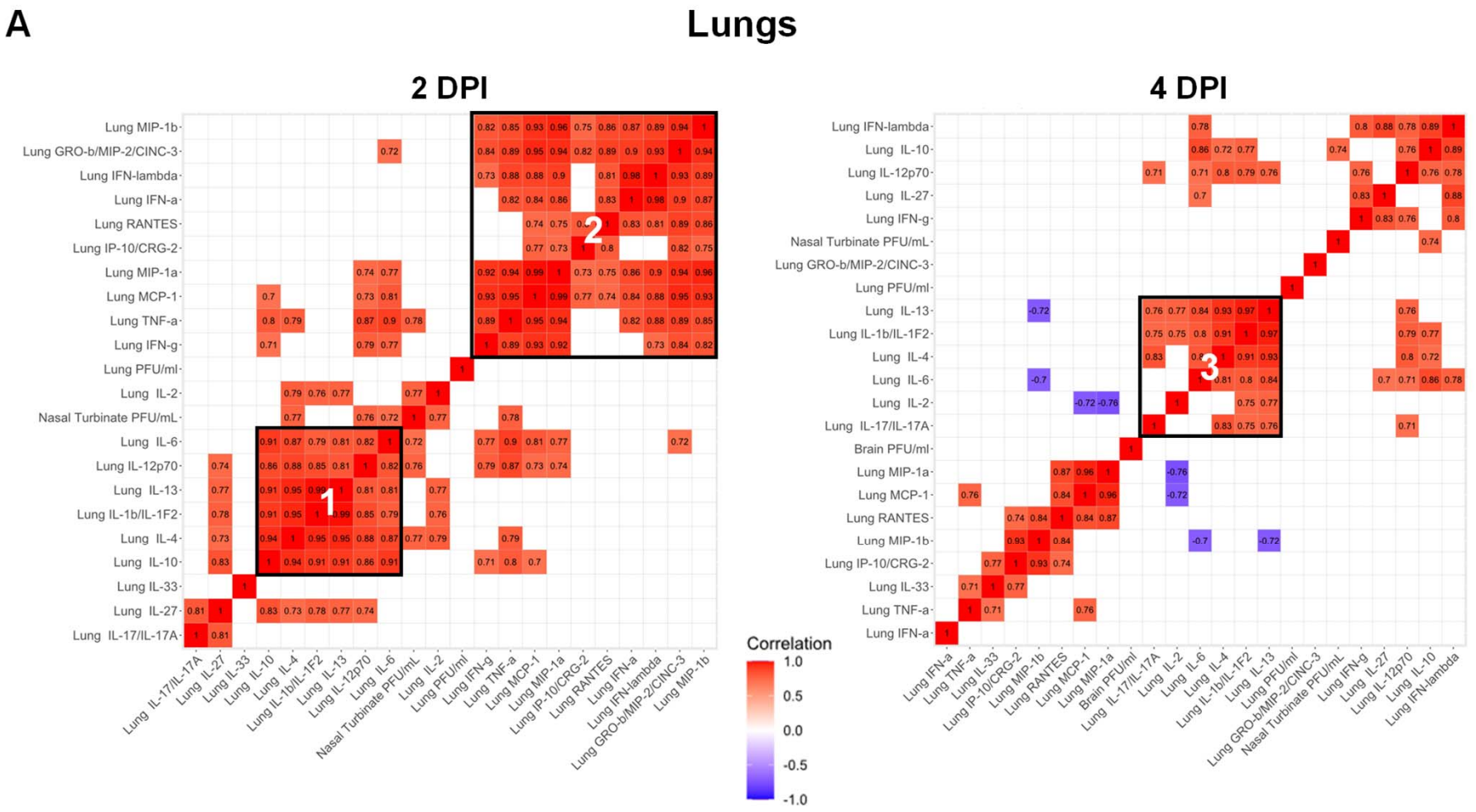

Figure 4. SARS-CoV-2 infected K18 hACE2 transgenic mice reveal differentiated clusters of chemokine and cytokine correlations with clinical symptoms progression. Hierarchically clustered Pearson correlations of measurements in (**A**) lung, (**B**) spleen and (**C**) brain of SARS-CoV-2 infected K18 hACE2 transgenic mice. Positive correlation (Red = 1) and negative correlations (Blue = -1), with clusters (Black outlined boxes with cluster number). Non-significant values ($p > 0.05$ measured by Pearson's correlation t-test) were left blank. DPI: Days post-infection. MIP-2/CXCL2; MCP-1/CCL2; MIP-1a/CCL3; MIP-1b/CCL4; RANTES/CCL5; IP-10/CXCL10.

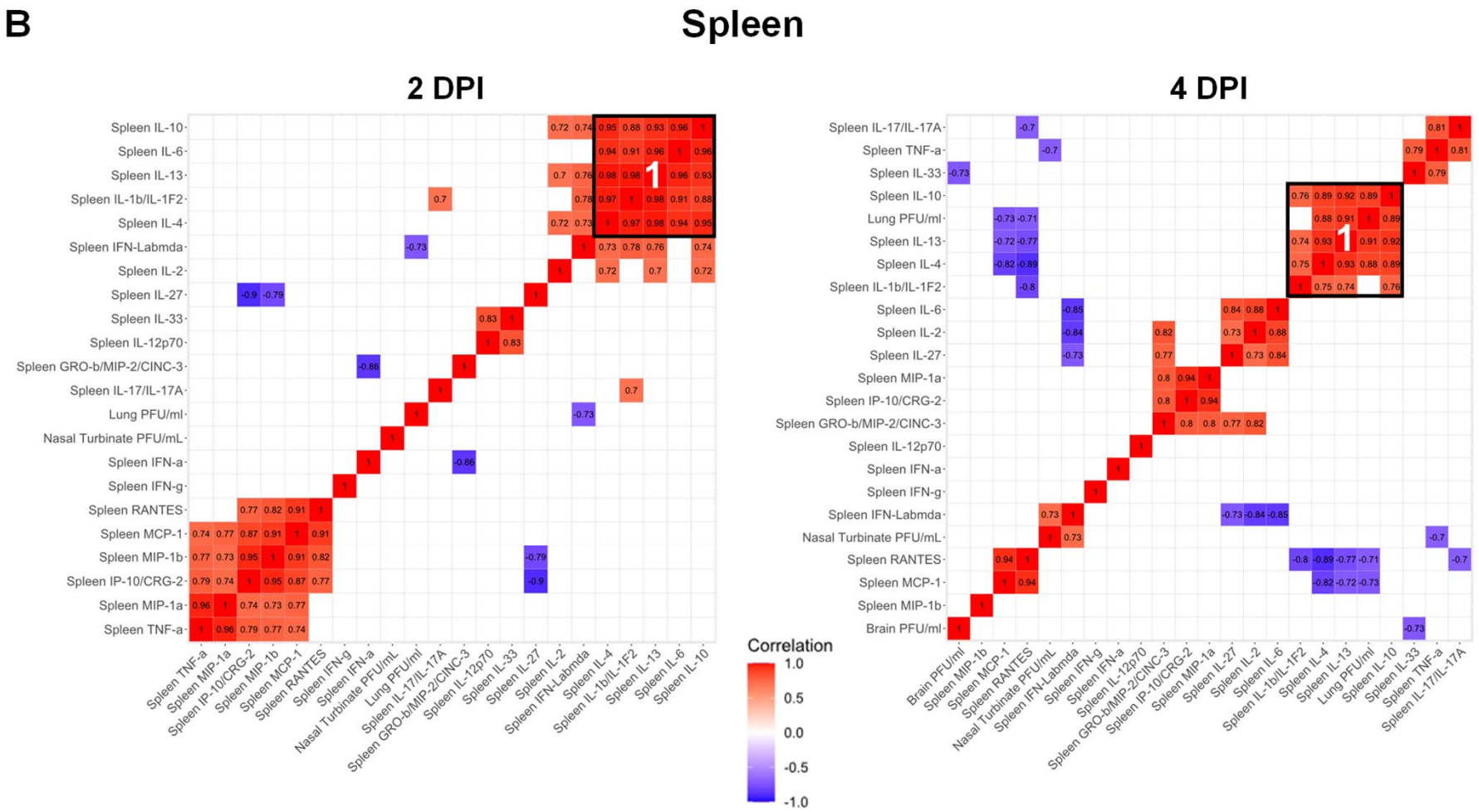

Figure 4. Continuation.

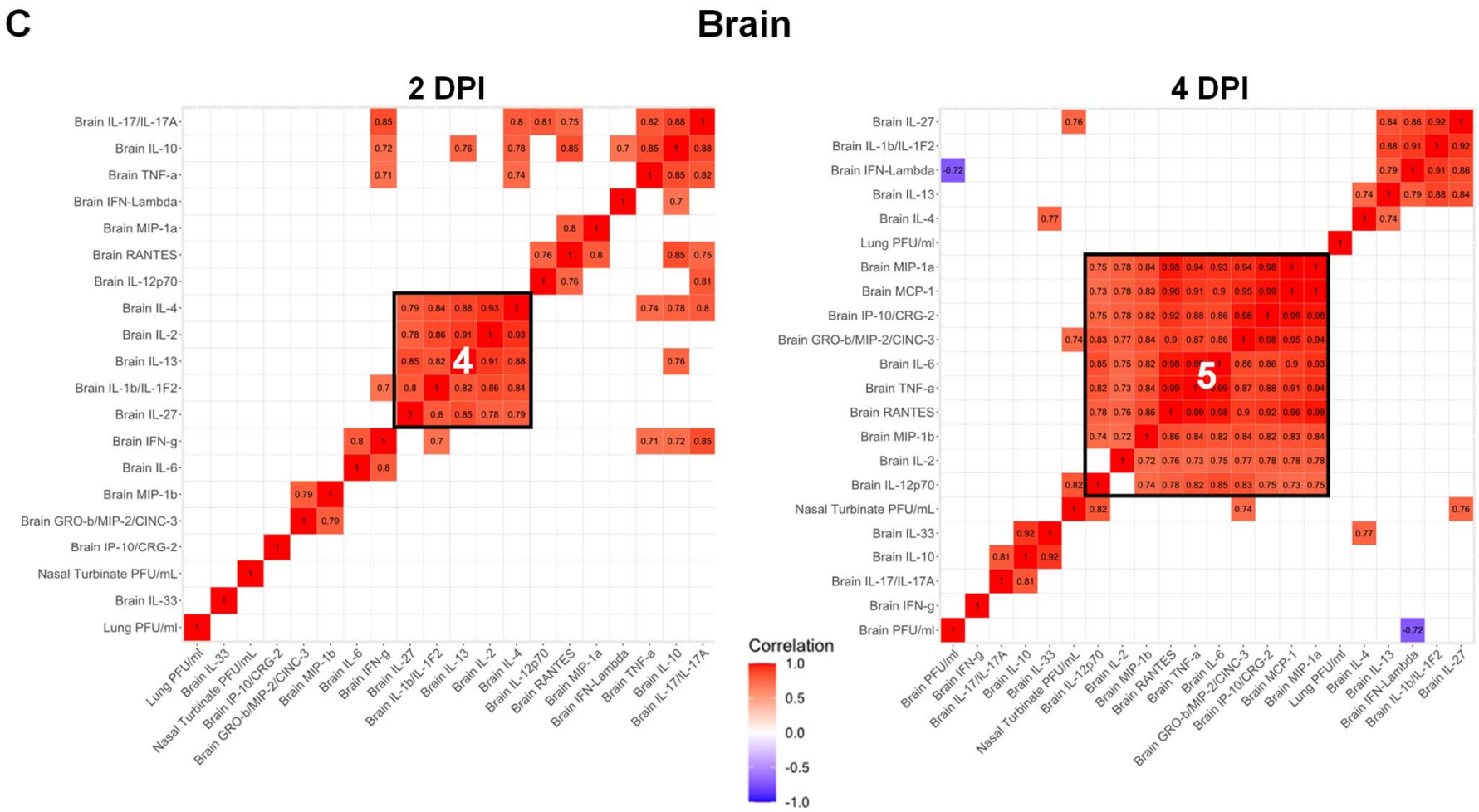

Figure 4. Continuation.

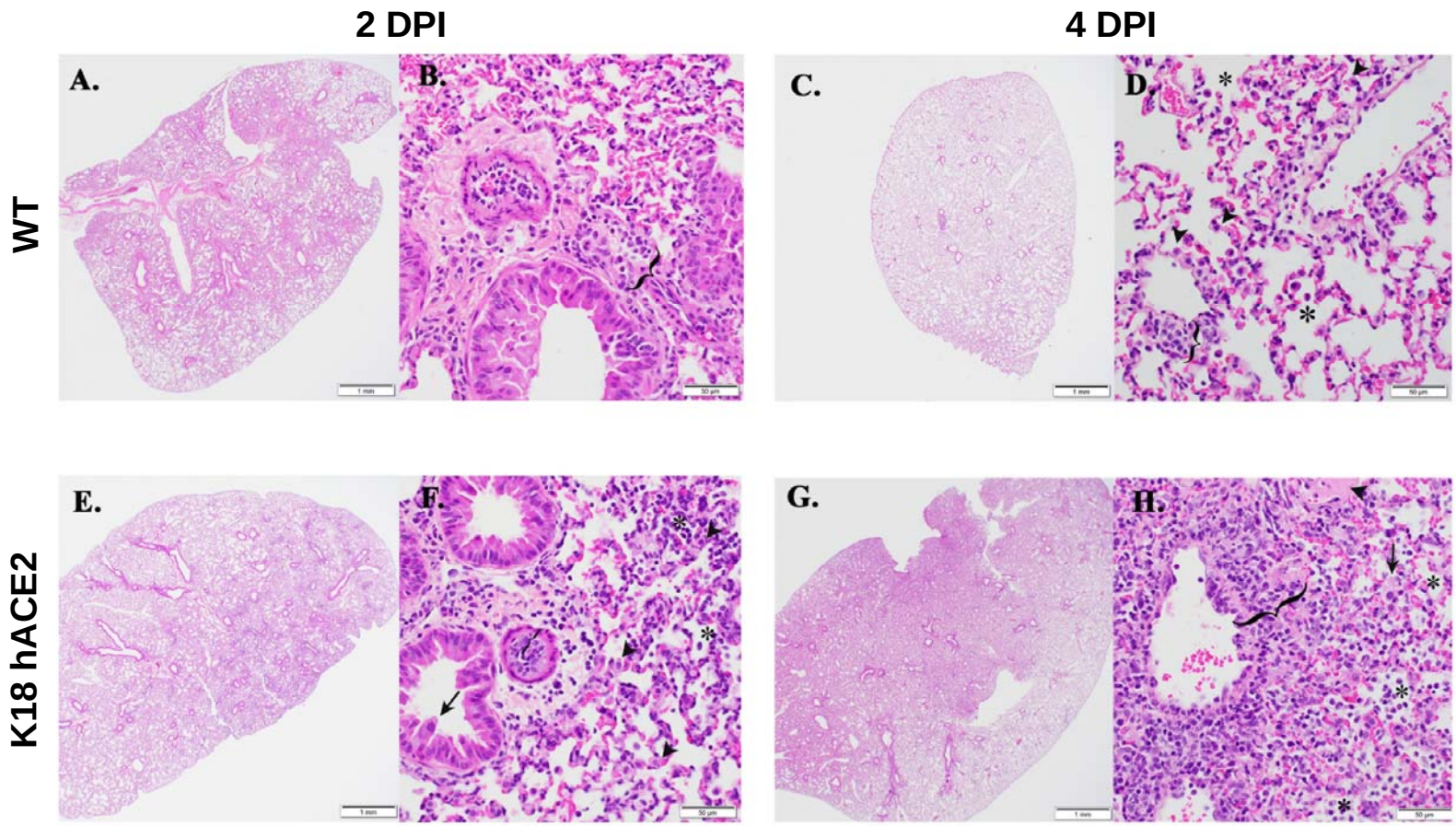

Figure 5. K18 hACE2 transgenic mice develop rhinitis, pneumonia with associated pulmonary inflammation after infection with SARS-CoV-2. (A-D and **I-L) WT C57BL/6 mice**. Minimal mononuclear and neutrophilic interstitial pneumonia in WT lung at 2-DPI (**A, B bracket**). By 4-DPI (**5C, D**) minimal alveolar histiocytosis (**D, asterisk**) pneumocyte type II cells (**D, arrowheads**), perivascular mononuclear inflammation (**D, bracket**) and rhinitis with low numbers of neutrophils (**K, arrowhead**) were variably observed. Lymphocyte aggregates in the lamina propria of the small intestine (**I, asterisk**). Mixed mononuclear inflammation with individual hepatocellular necrosis (**J, arrowhead**). Brain from WT 4-DPI was normal (**L**). **(E-H** and **M-P) K18 hACE2 transgenic mice**. Interstitial pneumonia (**E, F**) associated with alveolar histiocytosis admixed neutrophils and lymphocytes (**F, asterisks**), mild type II pneumocyte hyperplasia (**F, arrowhead**), bronchiolar syncytia (**F, arrow**), endothelial cells hyperplasia and vasculitis (**F, bracket**) by 2-DPI. Gut associated lymphoid tissue (GALT) with prominent germinal centers was observed (**M, asterisk**). Liver inflammation with variable amounts of individual hepatocellular necrosis (**N, arrowhead**). Greater lung involvement indicative of pneumonia (**G**), with inflammatory cellular accumulations and hemorrhage in alveolar spaces (**H, asterisk**) and interstitium (**H, bracket**), intra-alveolar fibrin admixed cellular debris (**H, arrow**), vasculitis (**H, bracket**), edema (**H, arrowhead**) by 4-DPI. Neutrophilic rhinitis observed at 4-DPI (**O, bracket**). Mild meningoencephalitis with vasculitis (**P, arrowhead**). Scale bars left images, 1 mm. Scale bars right images, 50 mm. DPI: Days post-infection.

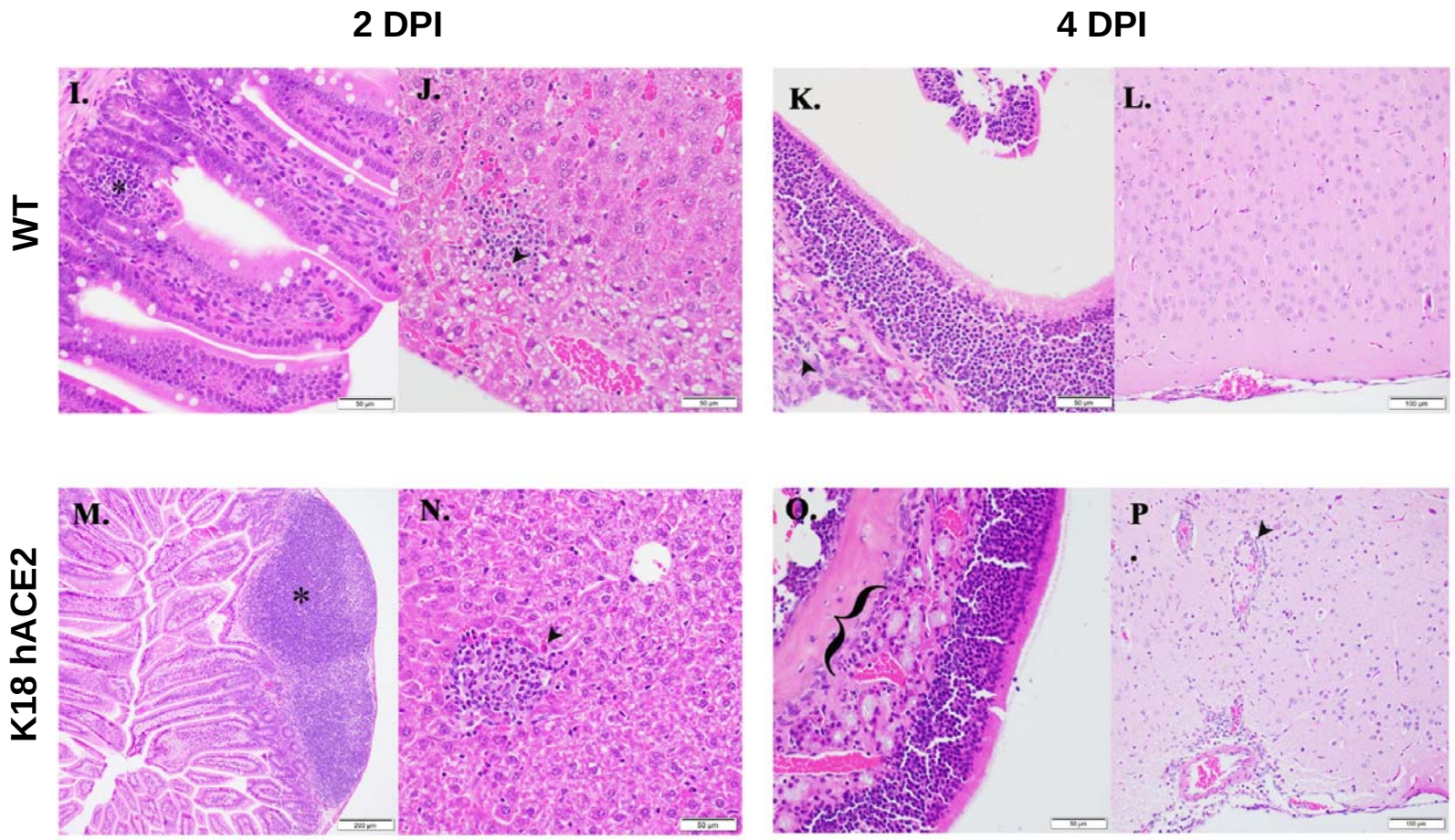

Figure 5. Continuation.

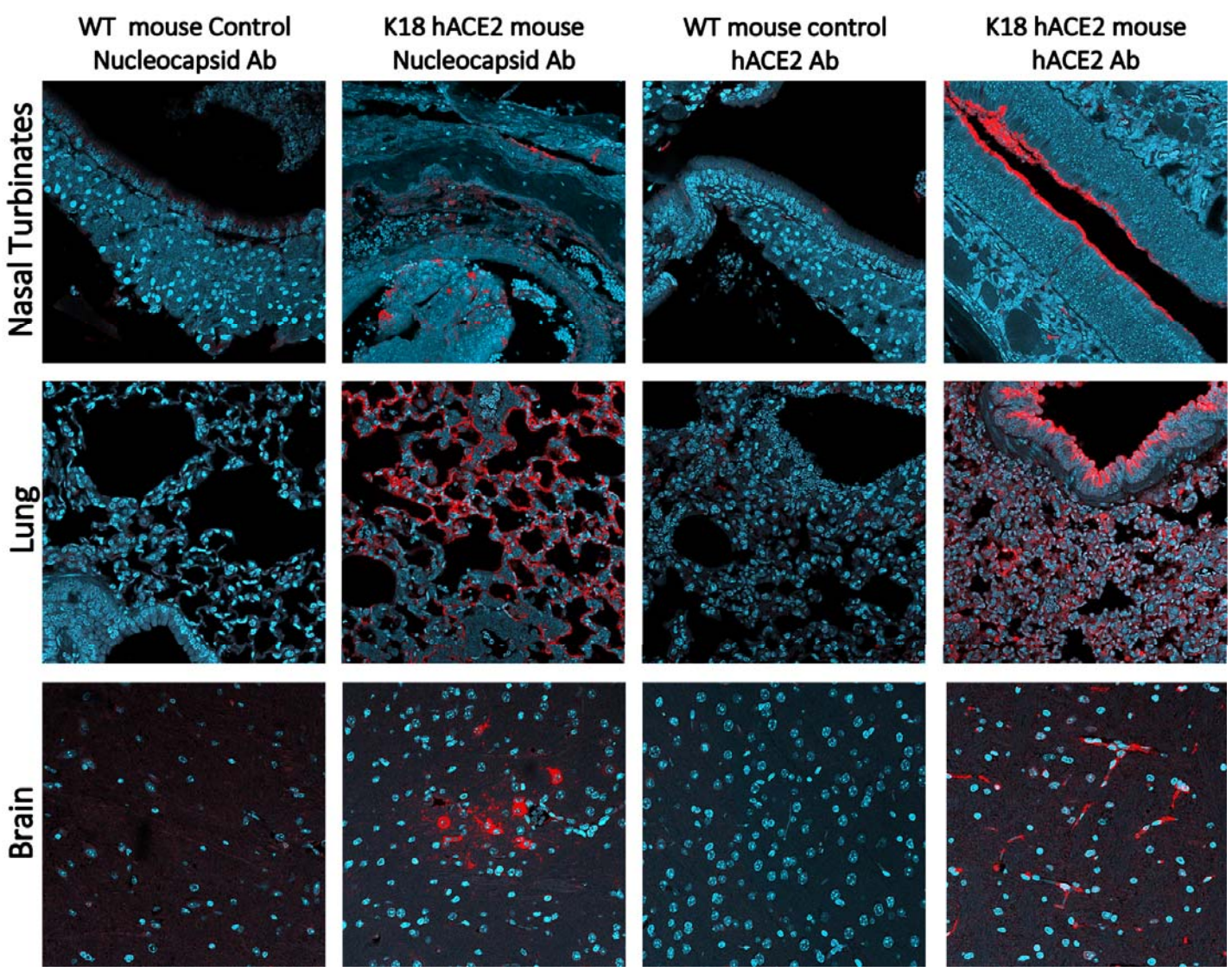

Figure 6. IHC examination of tissue from K18 hACE2 transgenic and WT C57BL/6 mice infected with SARS-CoV-2. (**A**) WT and K18 hACE2 transgenic C57BL/6 mice nasal turbinate (top, at 2-DPI), lung tissue (middle, at 2-DI) and brain (bottom, at 4-DPI) stained with an antibody against SARS-CoV-2 NP (red) or with antibody recognizing hACE2 receptor (red). (**B**) Infected choroid plexus in the brains of SARS-CoV-2-infected K18 hACE2 transgenic mice at 4-DPI. Left panel show that the hACE2 receptor (red) is highly expressed in the choroid plexus (all nuclei shown in aqua-blue). Right panel shows that some cells in the choroid plexus are infected with SARS-CoV-2 as these are positive to a SARS-CoV-2 NP (in red).

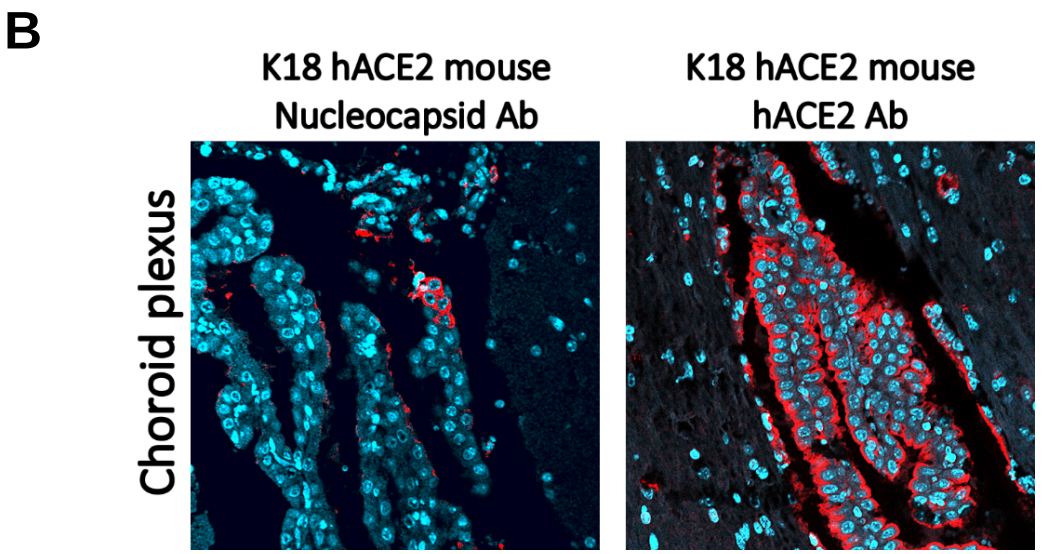

Figure 6. Continuation.